NAVAL POSTGRADUATE SCHOOL
Monterey, California

THESIS

ANALYSIS OF FINITE PHASED ARRAYS ON SHAPED GROUND PLANES

by

Ioannis E. Daniil

December, 1997

Thesis Advisor: David C. Jenn
Second Reader: Phillip E. Pace

Approved for public release; distribution is unlimited.

REPORT DOCUMENTATION PAGE

Form Approved OMB No. 0704-0188

1. AGENCY USE ONLY *(Leave blank)*	2. REPORT DATE	3. REPORT TYPE AND DATES COVERED
	December 1997	Master's Thesis

4. TITLE AND SUBTITLE
ANALYSIS OF FINITE PHASED ARRAYS ON SHAPED GROUND PLANES

5. FUNDING NUMBERS

6. AUTHOR(S)
Daniil, Ioannis E.

7. PERFORMING ORGANIZATION NAME(S) AND ADDRESS(ES)
Naval Postgraduate School
Monterey, CA 93943-5000

8. PERFORMING ORGANIZATION REPORT NUMBER

9. SPONSORING / MONITORING AGENCY NAME(S) AND ADDRESS(ES)

10. SPONSORING / MONITORING AGENCY REPORT NUMBER

11. SUPPLEMENTARY NOTES
The views expressed in this thesis are those of the author and do not reflect the official policy or position of the Department of Defense or the U.S. Government.

12a. DISTRIBUTION / AVAILABILITY STATEMENT
Approved for public release; distribution is unlimited.

12b. DISTRIBUTION CODE

13. ABSTRACT *(maximum 200 words)*

The objective of this thesis is to evaluate the performance of an array antenna when it is installed on an complex structure, such as those that have unusual edge contours, curved surfaces, and mixed material composition. A dipole is used as the basic array element to study the effect of various changes in the array design parameters on the gain and sidelobe level. Data is generated using a computational electromagnetics code based on the method of moments. Among the issues addressed are the curvature of the array ground plane and shaping the ground plane edges to reduce wide angle sidelobes.

14. SUBJECT TERMS
Arrays, Radiation Pattern

15. NUMBER OF PAGES
102

16. PRICE CODE

17. SECURITY CLASSIFICATION OF REPORT	18. SECURITY CLASSIFICATION OF THIS PAGE	19. SECURITY CLASSIFI- CATION OF ABSTRACT	20. LIMITATION OF ABSTRACT
Unclassified	Unclassified	Unclassified	UL

NSN 7540-01-280-5500

Standard Form 298 (Rev. 2-89)
Prescribed by ANSI Std. 239-18

Approved for public release; distribution is unlimited

ANALYSIS OF FINITE PHASED ARRAYS ON SHAPED GROUND PLANES

Ioannis E. Daniil
Lieutenant, Hellenic Navy
Hellenic Naval Academy, 1989

Submitted in partial fulfillment of the
requirements for the degree of

MASTER OF SCIENCE IN ELECTRICAL ENGINEERING

from the

NAVAL POSTGRADUATE SCHOOL
December 1997

ABSTRACT

The objective of this thesis is to evaluate the performance of an array antenna when it is installed on a complex structure, such as those that have unusual edge contours, curved surfaces, and mixed material composition. A dipole is used as the basic array element to study the effect of various changes in the array design parameters on the gain and sidelobe level. Data is generated using a computational electromagnetics code based on the method of moments. Among the issues addressed are the curvature of the array ground plane and shaping the ground plane edges to reduce wide angle sidelobes.

TABLE OF CONTENTS

ACKNOWLEDGMENT

This thesis is dedicated to my wife Athina for her understanding and support.

I. INTRODUCTION

A. BACKGROUND

Antennas are an important part of all radar and communication systems. In most cases, an antenna's performance is affected by the environment in which it is operating. The geometry and composition of the structure in which the antenna is installed, i.e. the platform, must be considered in its design to insure that the desired performance is achieved. [Ref. 1]

The main objective of this thesis is to evaluate the performance of an array antenna when the ground plane is serrated or curved, which would occur when installed on a complex structure. By a complex structure it is meant one that has edges and surfaces that may be doubly curved. The materials may include conductors and insulators such as composites. It is obvious that we need a much more accurate model for an array antenna in such real conditions than one for an antenna mounted in an infinite ground plane with the properties of a perfect electric conductor.

The purpose of this study is to investigate the effects of the antenna platform on the figures of merit that characterize the performance of the antenna. Primarily, they include the antenna gain and sidelobe level. This research

is performed by computer simulation using a code named **patch**[1]. [Ref. 4]

The computer modeling has the advantage of being more efficient and far less expensive than trying to test a design with hardware. State-of-the-art computer codes such as **patch** can accurately model edges, corners or even curved geometry (instead of flat surfaces), as well as materials with surface impedance (rather than perfect electric conductors) used in the construction of aircraft. Obviously, future design changes, both in the radar antenna and the aircraft, can be evaluated with less cost by using a computer simulation than by using hardware development models.

Modern, high performance radars and communication systems generally employ phased array antennas. In the past, printed circuit dipoles and slots have been used as radiating elements. Recently microstrip patches have been used because of their low profile, light weight and compatibility with integrated circuit fabrication techniques. This thesis research assumes that the traditional dipole is used as the basic array element. The research results can be extended to include other linearly polarized elements such as microstrip patches.

---

[1] Throughout the thesis lower case bold characters are used for computer code names.

In order to design and install the dipole array on the aircraft and obtain the predicted characteristics, we start from the very basic case of a single dipole, and then extend the analysis to the whole array by gradually increasing the number of elements. An important consideration in the array design is the ground plane: its location, conductivity and shape. In particular, the shape of the ground plane affects the sidelobes of the pattern and this becomes apparent when arrays of various geometries are examined.

A second objective of this study is to examine the individual patterns of the array elements so as to provide an understanding of the contribution of each element in the formation of the beam pattern. Each element's radiation pattern depends on its location in the array due to mutual coupling. Mutual coupling is a function of element dimensions, spacing, scan angle and ground plane spacing. Mutual coupling is taken into account in the array design; however, tuned elements that rely on strong mutual coupling will experience a correspondingly strong "edge effect." This can be a problem if the wide-angle sidelobes must be controlled. A second source of the edge effect is the termination of the ground plane. Diffraction at the ground plane edges also contributes to wide-angle sidelobe increase. As part of this study, we look at shaping the ground plane as a means of reducing the wide-angle sidelobes. In addition to radiation pattern changes, the

gain of the antenna must also be considered. The gain is perhaps the most important indicator of the overall array performance. The gain is calculated by numerical integration of the radiation pattern.

B. APPROACH

The antenna research is based on the use of a computer code named **patch**. It is a computational electromagnetics code that solves the E-field integral equation by the method of moments procedure. The antenna surfaces are discretized into subsections of triangular shape. The discretized (or faceted) body can be generated by a pre-processing code named **build** or by computer aided design (CAD) software such as **AutoCAD**. Additionally, in order to have an accurate estimation of the radiation pattern, the maximum length of the edges which are used should be less than 0.1λ. A separate program named **pchgain** computes the antenna gain using the currents generated by **patch**.

In order to be able to view the array geometry, the code **bldmat** is executed to generate MATLAB *.m files that are readable by the MATLAB script **pltpatch**. Information such as the edge number, the node number or the face number can be displayed. In this way, it is possible to specify the excitation points on the dipoles.

The computer model can be modified to vary the number of dipole elements, the dimensions, the shape and even the

conducting properties of the ground plane. The optimum dipole element is 0.45λ long where λ is the wavelength. For planar arrays, the ground plane is in the $x-y$ plane and the dipole is at a height of 0.15λ above the plane. When a finite ground plane is used instead of an infinite one the basic design guideline is to extend the ground plane at least 0.5λ farther than the outermost element.

To summarize, the following array design parameters where examined to determine their effect on array performance: ground plane extent and shape, number of elements and spacing, and ground plane curvature. In the last case it was found that the defocusing of the beam due to the array curvature could be reduced significantly by adding phase corrections. In all cases it is assumed that the ground plane is perfectly contucting.

C. THESIS OUTLINE

In addition to this introduction, this thesis includes five more chapters. Chapter II contains a description of different types of radiation elements and arrays in order to establish a theoretical background and a base of comparison and evaluation of the computed data. Chapter III is a brief description of the **patch** program. The method of moments and its corresponding implementation in the computer code is discussed. The entire simulation process involves several codes and the inter-relationships between them are defined.

Chapter IV presents the computer generated data as described in the previous section also details the array configurations investigated and includes pattern and gain data. Finally, Chapter V presents some conclusions based on the simulated array data.

II. RADAR ANTENNAS AND PERFORMANCE MEASURES

A. ANTENNA CHARACTERISTICS

For the particular antenna application of interest here, i.e., search and tracking radar, the antenna must concentrate radiated energy into a narrow beam and accurately point it in the target direction. Thus, radar antennas are typically directional antennas, providing sufficient gain in order to detect a target and the direction pointing accuracy for angular resolution of the observed targets in angle.

The discussion begins by introducing a number of basic antenna parameters and their relationship to performance measures such as gain and sidelobe level. Both gain and sidelobe level are obtained from the radiation pattern. The radiation pattern is defined as the relative distribution of the far-field radiated power as a function of direction in space.

For the special case of an array of identical elements the radiation pattern can be reduced to the product of two factors. The first one is the element factor which corresponds to the pattern produced by an individual element in the array when only it is excited and all others are loaded. The second factor is the array factor. It represents the effect of combining the individual excitations of all

elements of the array. The element factor is generally assumed to be identical for all elements in the array, even though this is not exactly true for a finite array. The pattern of elements near the edges of the array are significantly different than those of elements in the center of the array due to mutual coupling.

A complete representation of the radiation pattern requires a three dimensional plot. However most of the important antenna characteristics are available from the principal E-plane and H-plane patterns. The principal plane patterns of a linearly polarized antenna are cuts of the radiation pattern in orthogonal planes containing the beam maximum. The orthogonal planes are chosen so that the electric and magnetic field vectors lie in them. The principal planes are illustrated in Figure 1.

Contour plots are a convenient way to visualize the spatial radiation distribution. Direction cosine space is a natural choice for the coordinate axes. A point in unit space $(r=1)$ in the direction θ, ϕ is specified by its projection on the $x-y$ plane at $u=\sin(\theta)\cos(\phi)$ and $v=\sin(\theta)\sin(\phi)$ as shown in Figure 2. The z direction cosine is $w=\cos(\theta)$.

A measure of the concentration of the radiated power in a particular direction is the directive gain. The maximum directive gain (the directivity) can be expressed mathematically as the ratio of maximum radiation intensity

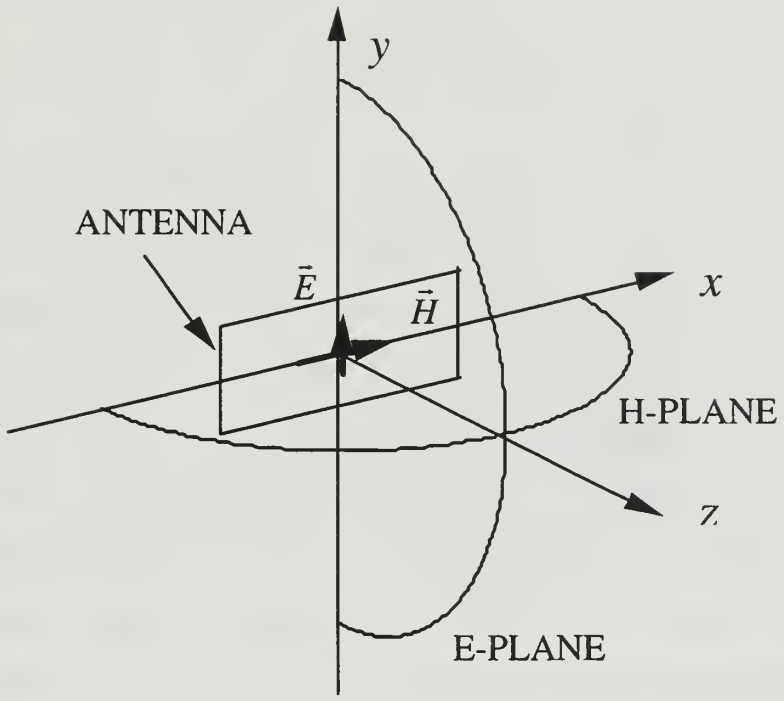

Figure 1. Definition of the principal planes of an antenna.

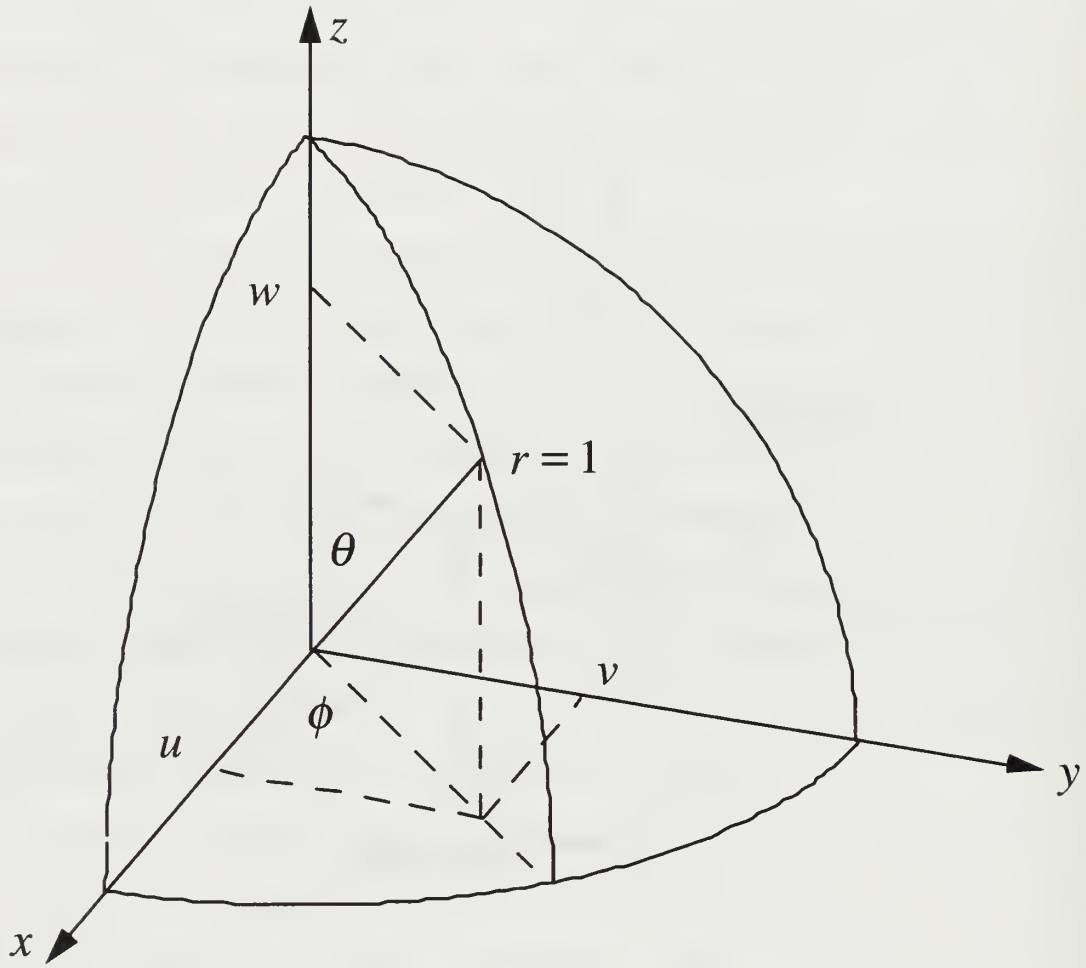

Figure 2. Definition of the direction cosines.

to the average intensity, or equivalently, the power radiated per unit solid angle in the direction of the maximum radiation over the average power radiated per unit solid angle:

$$D = 4\pi \frac{dP_r / d\Omega}{P_r}$$

where P_r is the total radiated power and $d\Omega$ is the differential solid angle in steradians.

Directivity does not take into the account losses that arise from imperfect conductors and lossy materials used in the construction of the antenna. The antenna power gain (or simply gain) is defined as the ratio of the power radiated per unit solid angle to the total input power, where the total input power includes not only the power radiated by the antenna but also the power dissipated within the antenna. Thus gain can be written as:

$$G(\theta,\phi) = eD(\theta,\phi)$$

where e is the antenna efficiency factor ($0 \le e \le 1$).

B. ANTENNA CLASSIFICATION

The most basic and probably the most commonly used antenna is the half-wave dipole. As its name implies, its length is half of the wavelength of the radiated time-

midpoint by a voltage source connected by a transmission line. In practice each of the antenna arms is slightly less than one-quarter wavelength long for resonance. According to the boundary conditions the current must vanish at the ends of the arms and as a result, the current distribution is usually approximated by a sinusoid. The resulting magnetic and electric fields in the far field can be expressed as

$$H_\phi = \frac{jI_o e^{-j\beta r}\cos\left(\frac{\pi}{2}\cos(\theta)\right)}{2\pi r\sin(\theta)}$$

$$E_\theta = \eta H_\phi \qquad (1)$$

where $\beta = \frac{2\pi}{\lambda}$, I_o the current amplitude and η the characteristic impedance of free space ($\approx 377\,\Omega$). The radiation pattern for the dipole is shown in Figure 3. A tuned (resonant) half-wave dipole antenna has a radiation resistance of about $73\,\Omega$.

Horizontal dipoles above a perfect ground plane are used to radiate horizontally polarized waves. Vertically polarized waves are obtained by using a dipole perpendicular to the conducting ground plane. However, by the method of images only half the dipole is physically required, the second half can be replaced by the ground plane image. This

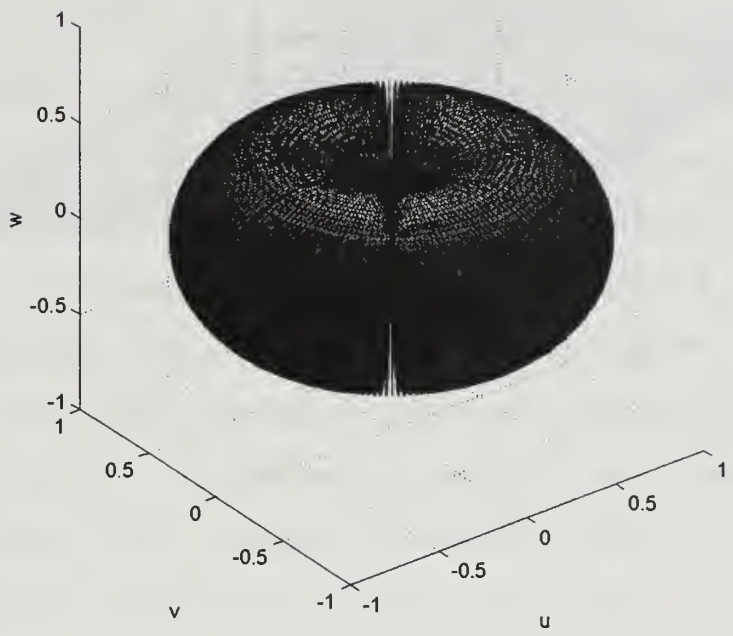

Figure 3. Radiation pattern for a single dipole.

monopole configuration is more compact than using a full dipole above the ground plane. A small loop antenna is referred to as the dual of the small dipole (the loop diameter is much smaller than the wavelength). The radiation pattern resembles that of the small dipole but the electric and magnetic field components are interchanged.

More complex radiating elements are used to generate circularly polarized fields. They include the helix, crossed dipoles and crossed slots. Over the past twenty years, microstrip patches have become more popular as both circularly and linearly polarized antennas. Patches are low profile and are easily fabricated using monolithic microwave integrated circuit techniques [Ref. 2]. A drawing of a rectangular microstrip patch is shown in Figure 4 [Ref. 3].

Arrays of basic radiators can be arranged geometrically and excited to provide a high gain antenna. In addition, arrays can be used to feed reflectors and lenses. The array illuminates a reflector which reflects and collimates the radiation in order to obtain a narrow secondary beam pattern. Reflector surface shapes include parabolic, spherical and other special profile reflectors. Some reflecting systems employ a single reflector, while others consist of a main reflector and one or more secondary subreflectors.

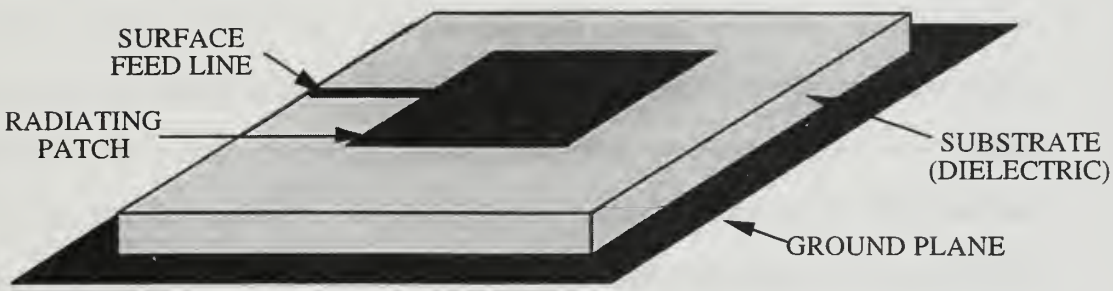

Figure 4. Example of a rectangular microstrip patch antenna fed for linear polarization.

A concept applicable to most large antennas is that of an aperture. The aperture is generally considered as a relatively flat surface through which all of the radiating power flows. For example, in the case of a circular parabolic reflector, the aperture would be a circle defined by the rim of the reflector. For a rectangular array it would be a rectangular surface with the array dimensions, slightly in front of the radiating elements.

Since many types of antennas can be reduced to an equivalent aperture antenna, a common theory can be used to model a wide range of antenna types. This is done by invoking the equivalence principle: the far-fields are uniquely determined by the tangential electric and magnetic currents flowing over the aperture.

For radar applications it is essential to design antennas with more energy radiated in some specific directions (i.e. towards the target) and less in other directions. Individual dipoles are rarely used as independent antennas and never as antennas for conventional radars[2]. However, antennas consisting of resonant half wavelength dipoles, usually assembled in rows and columns can be used. In order to obtain unidirectional radiation

---

[2] Low gain antennas such as dipoles are sometimes used in impulse radars.

pattern, a metallic reflector is located at a specific distance behind the dipoles.

The main type of array antenna used in radar applications is the phased array, where the beam pattern is controlled by the relative phases of the excitation coefficients of the radiating elements. Advantages include: (1) the ability to change beam position in space almost instantaneously by electronic scanning, (2) high directivity and gain, (3) ability to synthesize any desired radiation pattern including formation of pattern nulls in the direction of undesired interference sources, (4) the capability of very high powers from many sources distributed across the aperture and, finally, (5) the compatibility with digital computers and the use of digital signal processing. However, a significant drawback is that they are extremely complicated and as a consequence very expensive.

This research concentrates on arrays of simple half wave dipoles, which are convenient to model. The results can be extended to most other linearly polarized elements. In the next chapter the computer codes used to model the array are described.

III. COMPUTER CODE DESCRIPTION

A. GENERAL DESCRIPTION

Patch is a FORTRAN computer code that provides the ability to compute radar cross sections (RCS) as well as radiation patterns using the integration of surface currents [Ref. 4]. The calculation is based on a method of moments (MM) solution of the E-field integral equation (EFIE). In particular, when a perfect conducting scatterer is in presence of an impressed electric field $\bar{E}^i$, the integral equation is obtained by enforcing the boundary condition on the tangential component of the total electric field, which must be zero on the surface of the conductor:

$$\left(j\omega\bar{A}+\nabla\Phi\right)_{\tan}=\bar{E}^i_{\tan}$$

where

$$\bar{A}(\bar{r})=\frac{\mu}{4\pi}\int_S \bar{J}(\bar{r}')\frac{e^{-jkR}}{R}dS'$$

and

$$\Phi(\bar{r})=\frac{1}{4\pi\varepsilon}\int_S \sigma(\bar{r}')\frac{e^{-jkR}}{R}dS' .$$

Here S is the antenna surface over which the induced current density $\bar{J}$ flows, ε and μ are the permittivity and permeability of free space, $R=|\bar{r}-\bar{r}'|$ is the distance between

the source and the observation points $\bar{r}$ and $\bar{r}'$ respectively, and σ is the surface charge density.

To apply MM requires that a suitable triangular patch model of the geometry has been obtained using the code **build**. The method of moments reduces the electric field integral to a set of simultaneous linear equations that can be solved using standard matrix methods.

The surface current density $\bar{J}_S$ is represented as the sum of N terms; each term is the product of a known basis function and an unknown complex coefficient. Thus

$$\bar{J}_S(\bar{r}) \approx \sum_{n=1}^{N} I_n \bar{f}_n(\bar{r})$$

where $\bar{f}_n(\bar{r})$ are the basis functions and I_n the complex coefficients.

The number of unknowns N and, consequently, the size of the matrix equation that must be solved, depends on the number of triangle edges that are used to represent the given geometrical object. The area between edges which form the triangle facets is solid material. Therefore current flows on the surface of the object, not just along the edges of the triangles as would be the case for a wire grid model. As the triangles become smaller, the method of moments solution converges to the true value. Of course, there is a computer limitation as far as increasing the size of the matrix. The computer limits the number of unknowns and as a

result, the number of edges that can be used for the representation of the model. A general rule of thumb is that the triangle edge lengths should not exceed 0.1 wavelength.

Note that for the receive problem the current $\bar{J}_s$ must be recomputed at every new incidence angle. A concern is that for large matrices the computation time could be excessive. It turns out that the current distribution on the antenna is essentially the same for all incidence angles except for a phase shift. Thus it is more efficient to solve the corresponding transmit problem where the current only needs to be determined once.

B. INPUT FILE FOR PATCH

Upon execution, the **patch**[3] code reads an input file named **inpatch**. This is an ASCII file which contains the geometry information and the calculation parameters. In order to generate **inpatch** the code **build** is executed first. Subsequently, **patch** is executed, which performs the required current and radiation calculations. The results are posted in an ASCII output file called **outpatch.** The current coefficients are also posted in a file called **current**. This

[3] There are slight variations of each major code which are given individual names. For example, versions of **build** include **buildn5** and **builduv**. In the discussions that follow all of these are simply referred as **build**. Similarly, **patch** includes **patch2**,**pchfck** and **pchuv**.

allows further pattern and gain calculations without having to recalculate the currents.

As it has already been mentioned, the code **build** is used in this study to create the antenna geometry that is to be investigated, and also to specify the excitation conditions. This code provides the ability to include image symmetry planes of either perfect electric conductor or perfect magnetic conductor types placed in the $x=0$, $y=0$ or $z=0$ planes. Thus it is possible to compute the radiation pattern of an element over an infinite ground plane using this feature. The code provides the ability to examine both plane wave and voltage source excitations. For this particular research, it is more efficient to approach this as a transmit problem rather than a receive problem. By specifying such parameters as the number of voltage excitations and the triangle edges across which each voltage is applied, an array of radiators can be described. Each dipole can be excited with its own voltage in order to create the necessary phase differences to steer the array beam. Other features include lumped impedance loads and surface impedance loads.

After the antenna geometry has been defined **build** asks for input regarding the observation angles for pattern calculations. The radiation pattern angles are specified using the suitable ϕ and θ start and stop angles. For a

contour plot in direction cosine coordinates, a modified version of **patch** (**pchuv**) requests the start, stop and number of divisions in direction cosines u and v.

When **patch** completes its calculations, it writes ASCII data to several files. A summary of all the geometric and calculation parameters, including the values of the current distribution at each edge, is provided in **outpatch**. The current crossing the excited dipole edge which serves as the feed point is used along with the known excitation voltage to obtain the driving point impedance. This is illustrated in Figure 5. The current coefficients are also written to a file named **current** which is used subsequently to compute the gain. In addition to these two files there are four *.m files which can be loaded into MATLAB for pattern visualization.

The final step in computation of the array performance is to execute **pchgain**. It reads the previously generated **current** file. The file **outgaus** must be provided. It contains integration constants for Gaussian quadrature. The directivity is computed by numerically evaluating the formula

$$D = \frac{4\pi}{\Omega_A}$$

where

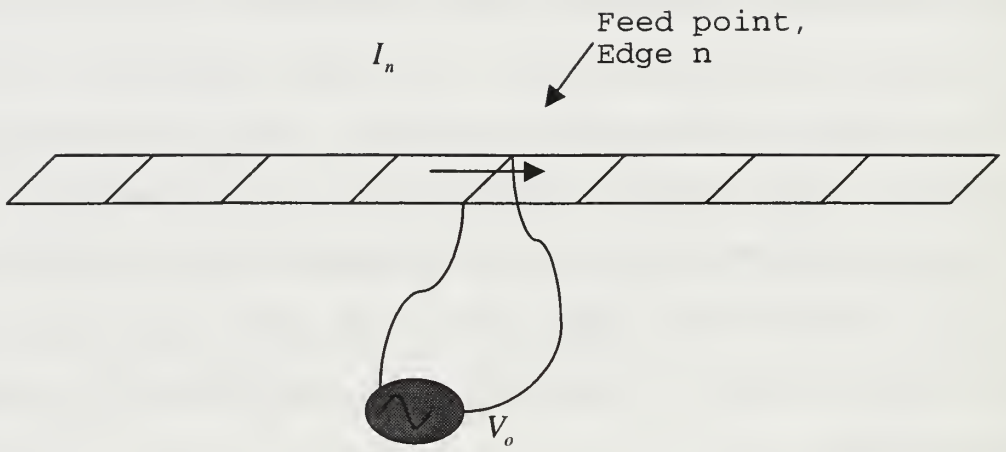

Figure 5. Example of voltage excitation for a dipole. The driving point impedance is $Z = V_o / I_n$.

$$\Omega_A = \frac{1}{\left|\bar{E}_{\max}\right|^2} \int_0^{2\pi} \int_0^{\pi} \left|\bar{E}(\theta,\phi)\right|^2 \sin(\theta) d\theta d\phi \ .$$

The pattern scales for the data presented in the following discussion are not normalized to the directivity. The values plotted are simply $20\log_{10}(\bar{E}(\theta,\phi))$ and therefore are labeled as "Power in dB."

In order to be able to display the antenna geometry the code **bldmat** is used to generate data files that can be loaded into MATLAB. The MATLAB script **pltpatch** displays the antenna in three dimensional space including labels for edge, node and face numbers if desired. Standard MATLAB commands can be used to rotate the object or zoom into a subset of the antenna. The relationship between the codes are illustrated in the flow chart in Figure 6. The next chapter presents data obtained using these codes.

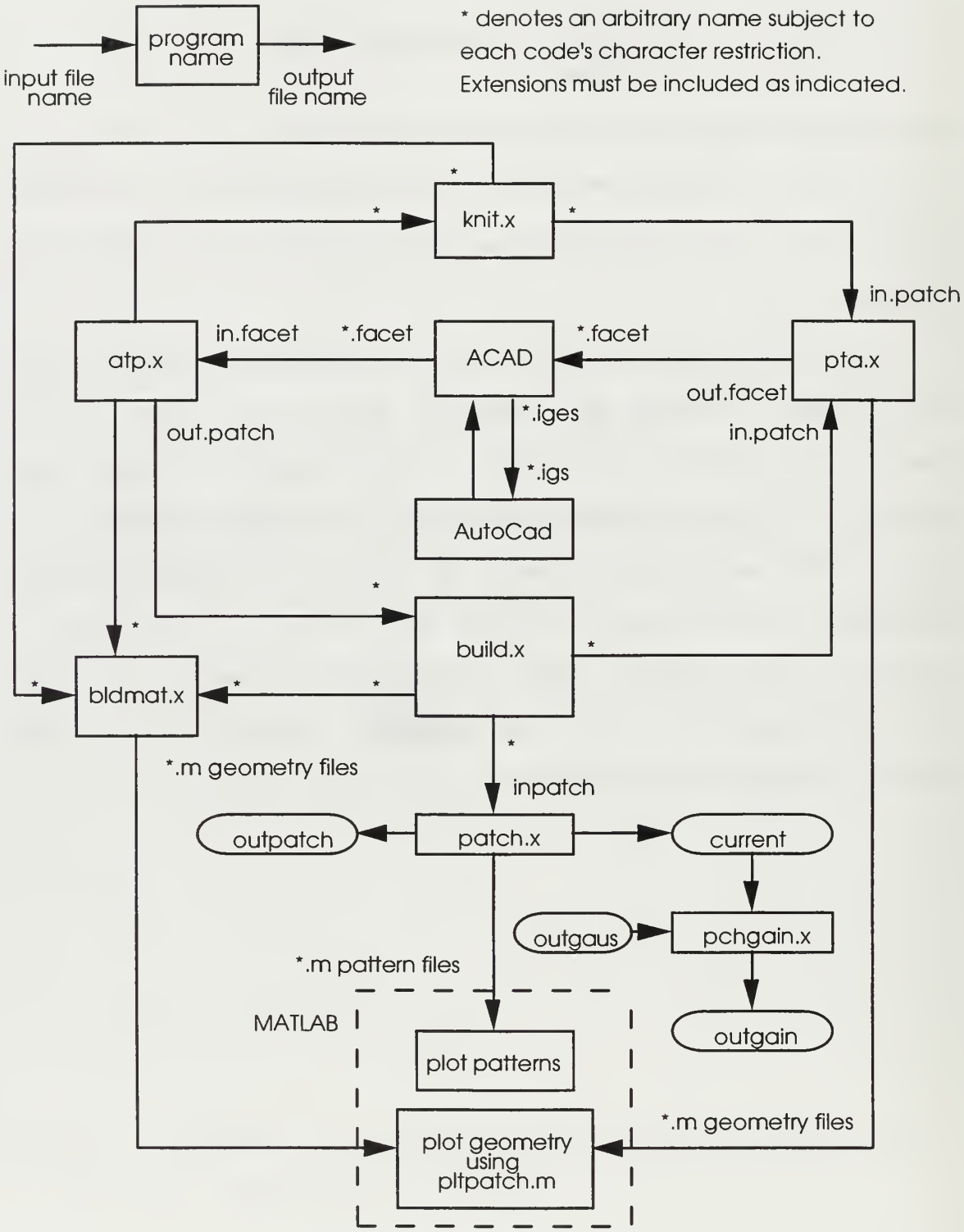

Figure 6. Flow chart illustrating the relationships between the various computer codes [Ref. 4].

IV. SIMULATION RESULTS

A. BASELINE CONGIGURATION

The computer study is based on calculating the performance of an array antenna by changing the design parameters one at a time. The parameters include the dimensions, shape, and material properties of the ground plane. For convenience the frequency of 300 MHz is chosen ($\lambda = 1\text{m}$). Therefore dimensions in meters are equal to dimensions in wavelength. The radiating element is a thin strip with length 0.45λ and width 0.025λ. The array ground plane is placed in the $x-y$ plane and the dipoles at a height of $z = 0.15\lambda$. A commonly used rule of thumb for determining the size of a finite ground plane is to have edges that extend 0.5λ farther than the outermost dipoles. The baseline array configuration is shown in Figure 7. The dipole spacing is 0.4λ in the H-plane and 0.55λ in the E-plane for the two-dimensional arrays.

In order to demonstrate the application of **patch** consider a single dipole. As illustrated in Figure 5 a voltage source of $V_o = 1e^{j0}$ V is placed at the edge that corresponds to the mid-point of the dipole. As shown in Figure 8 the radiation pattern for $\phi = 0$ (the E-plane) agrees with the analytical result given in Equation 1.

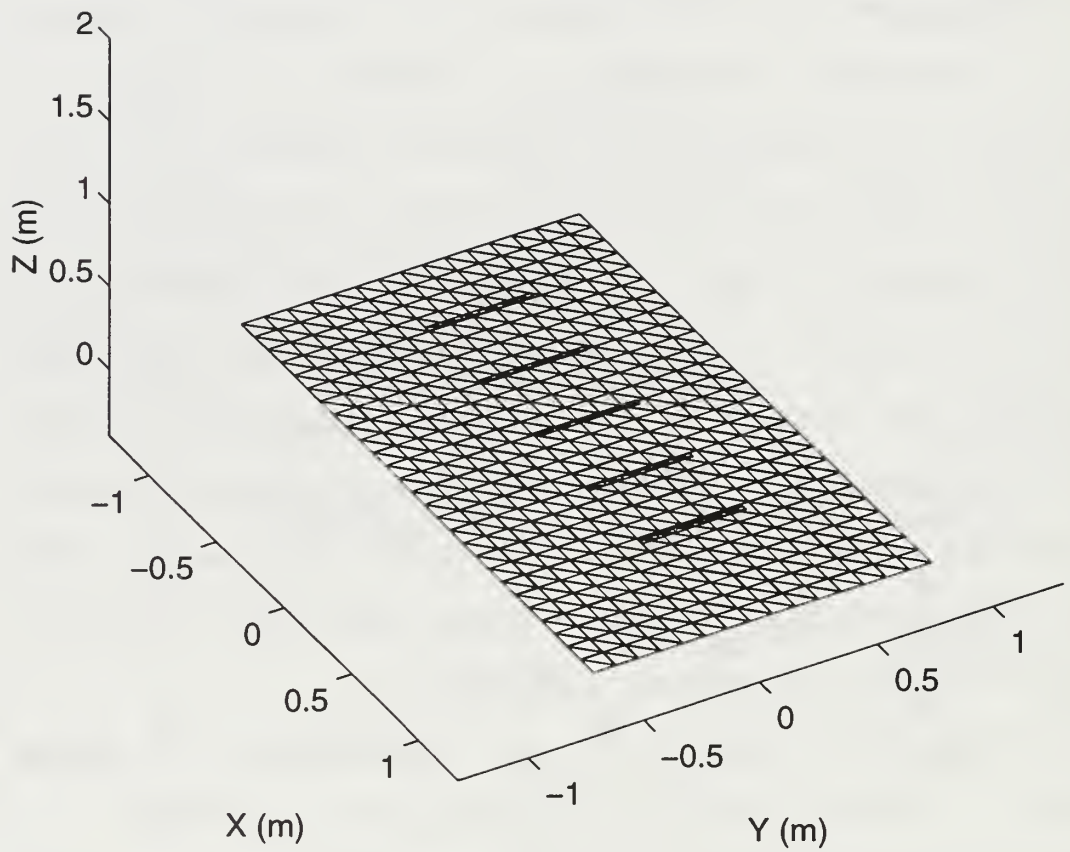

Figure 7. Five element array over finite ground plane.

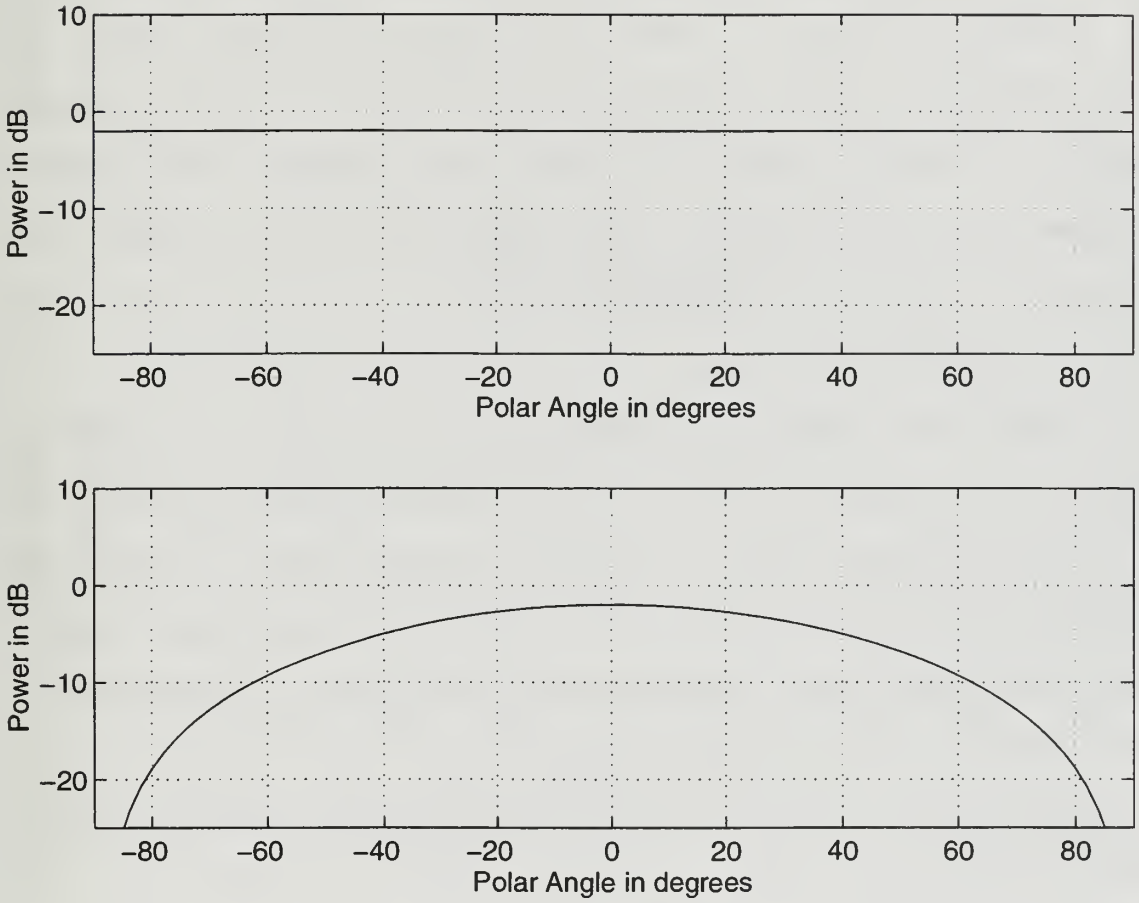

Figure 8. Radiation pattern for a single dipole obtained from **patch** (top: $\phi = 0^o$; bottom: $\phi = 90^o$).

The first step in this study is to examine the effect of the ground plane on the antenna pattern. The pattern of a dipole above an infinite ground plane is shown in Figure 9. If we indroduce a finite ground plane (still a perfect electric conductor) on the $x-y$ plane, with dimentions 1.45 by 1.025 wavelengths (Figure 10), then the radiation pattern is shown in Figure 11. The beam characteristics near $\theta = 0$ are essentially the same for the finite and infinite ground planes. However, scattering from the ground plane edges increases the pattern at wide angles ($\theta \geq 70^{o}$). Also, the field in the rear hemisphere ($\theta > 90^{o}$) is non-zero for the finite ground plane case.

Next, the number of elements is increased to three as shown in Figures 12 and 13. The distance between dipoles is 0.4λ. The pattern for the infinite ground plane is shown in Figure 14. Due to the fact that two dipoles have been added, the array gain has increased and sidelobes introduced. If the infinite ground plane is replaced with a finite plane with dimensions 1.45 by 1.825 wavelengths, the wide angle pattern does not drop to zero as seen in Figure 15. The array is increased to five elements, Then the radiation pattern for infinite and finite ground planes are shown in Figures 16 and 17 respectively.

Finally, the radiation resistances are calculated for each of the dipoles that have been examined so far. As

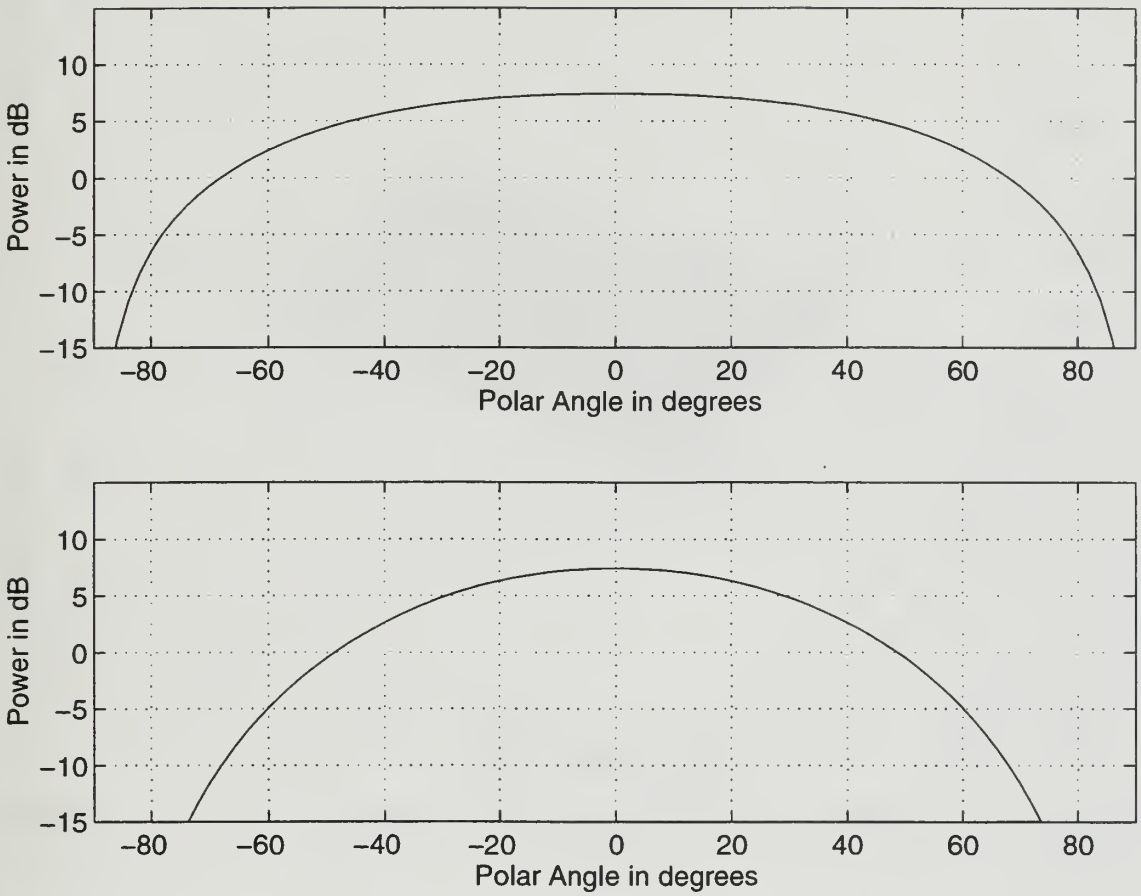

Figure 9. Radiation pattern for single dipole over infinite ground plane obtained from **patch** (top: $\phi = 0^o$; bottom: $\phi = 90^o$).

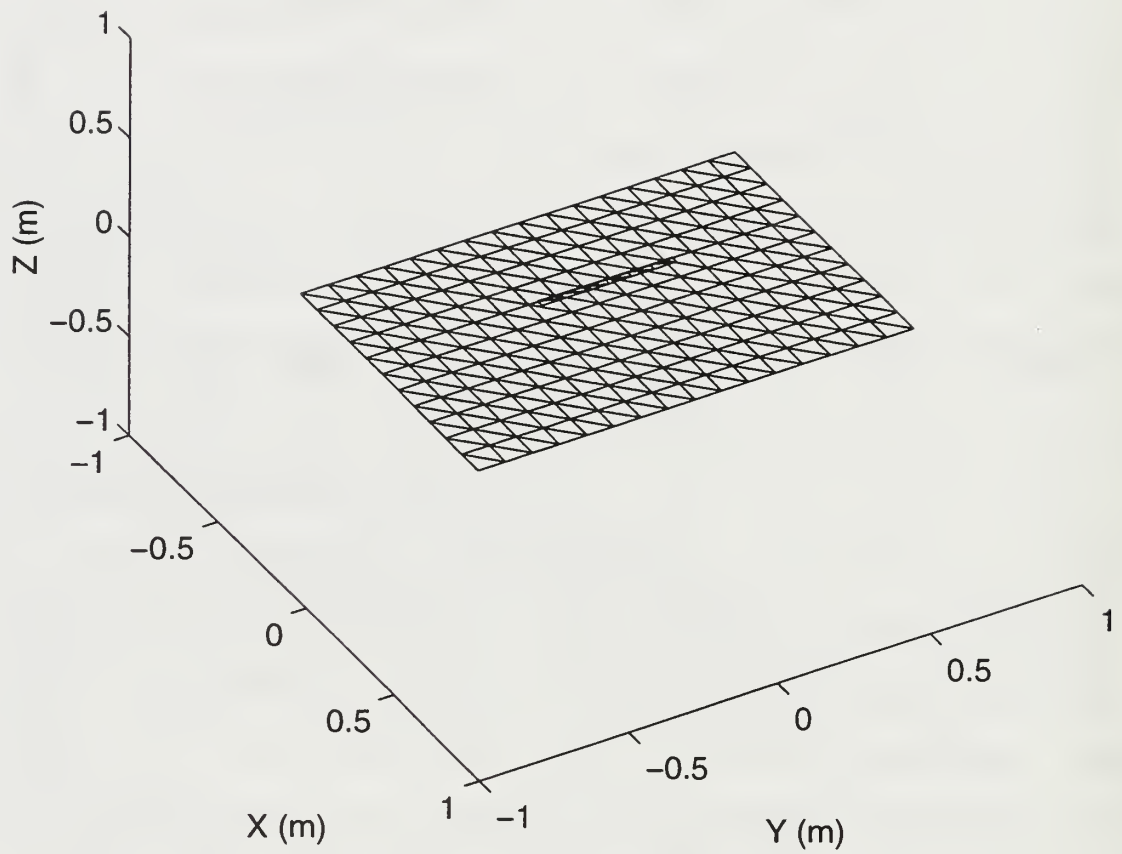

Figure 10. Single dipole over finite ground plane.

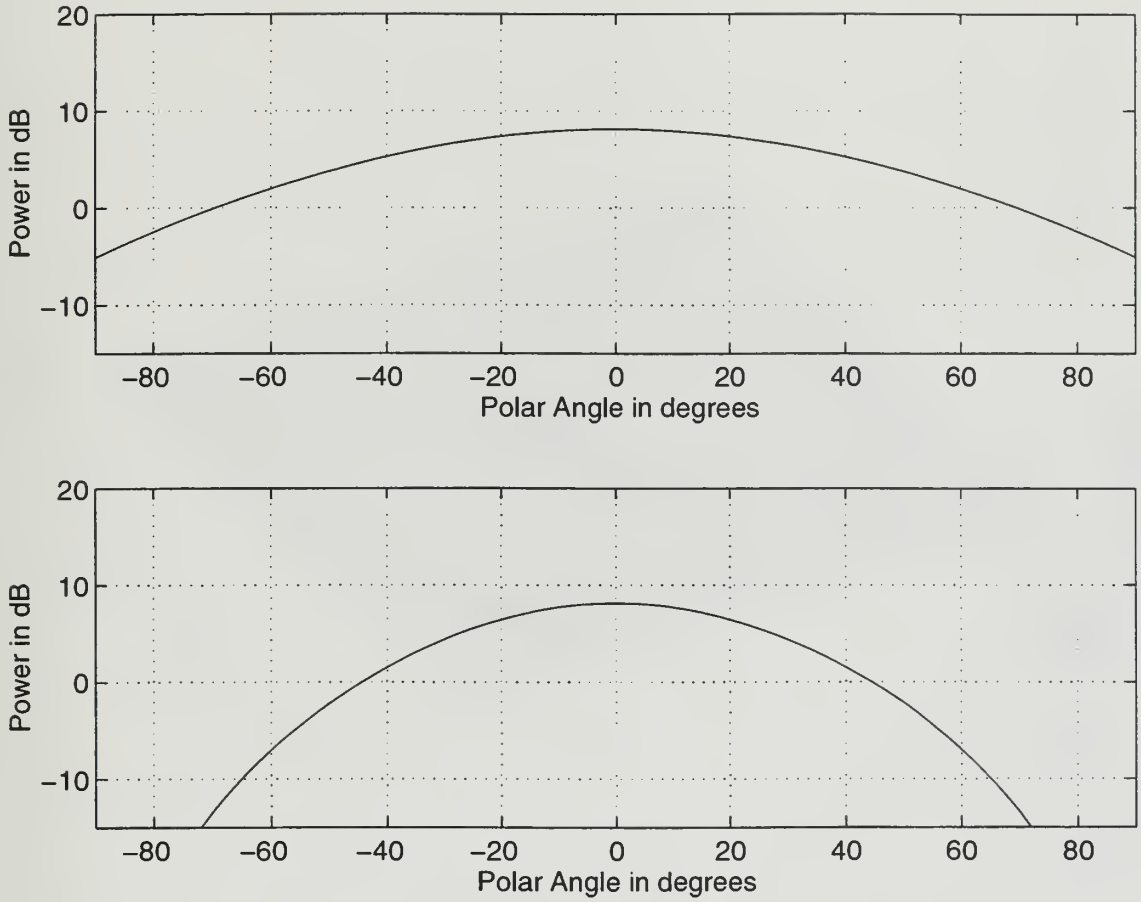

Figure 11. Radiation pattern for a single dipole over finite ground plane obtained from **patch** (top: $\phi = 0^o$; bottom: $\phi = 90^o$).

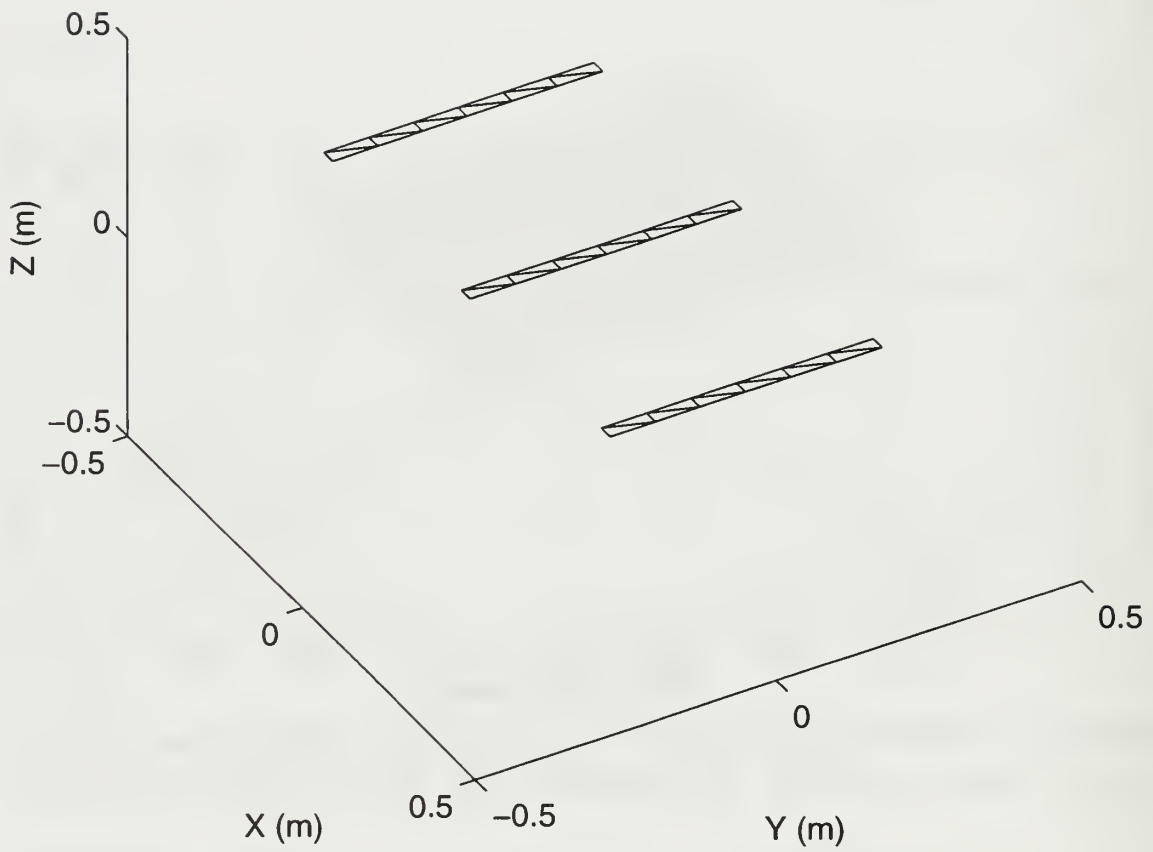

Figure 12. Three element array over an infinite ground plane.

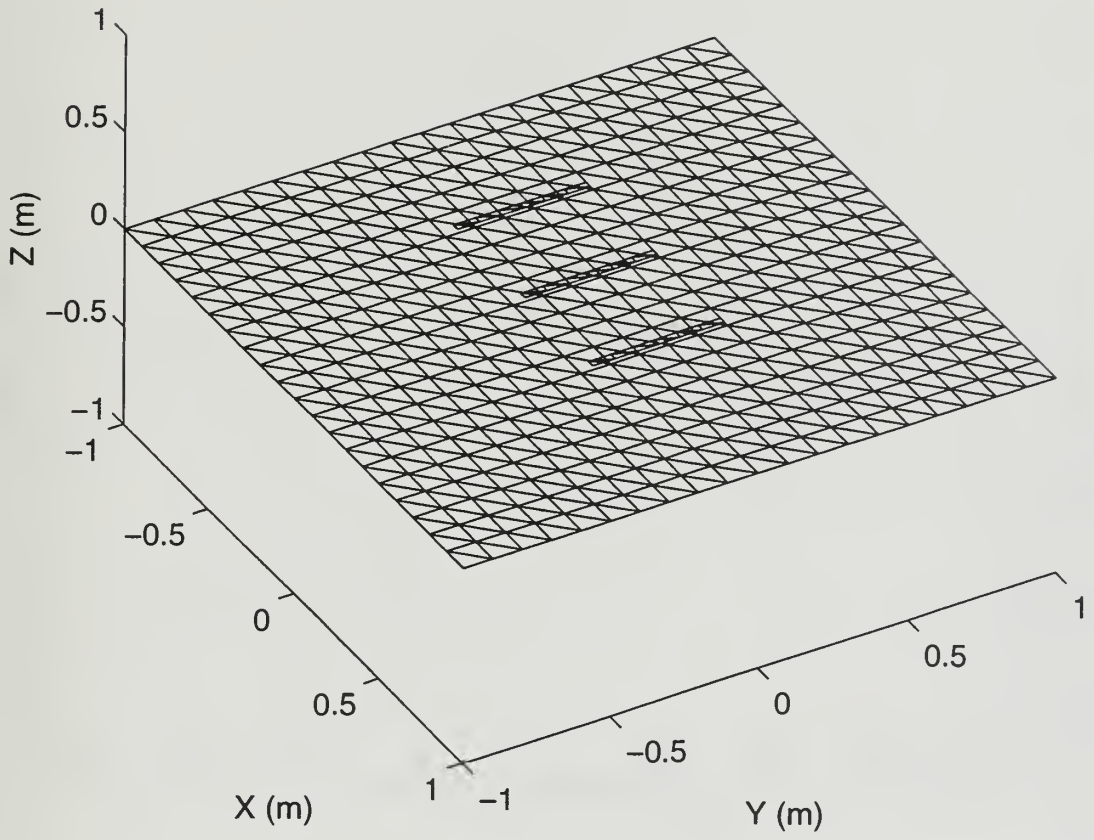

Figure 13. Three element array over a finite ground plane.

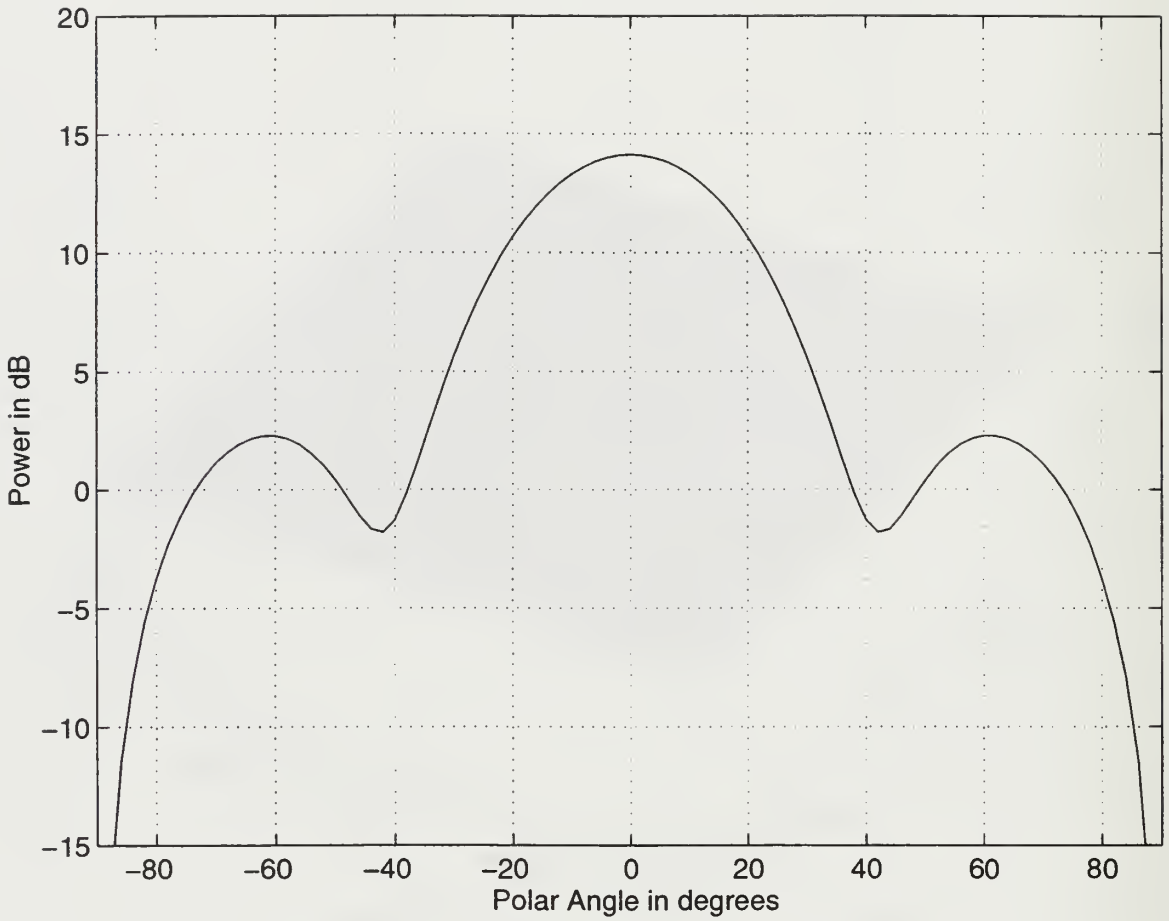

Figure 14. Radiation pattern for three elements over an infinite ground plane ($\phi = 0^o$).

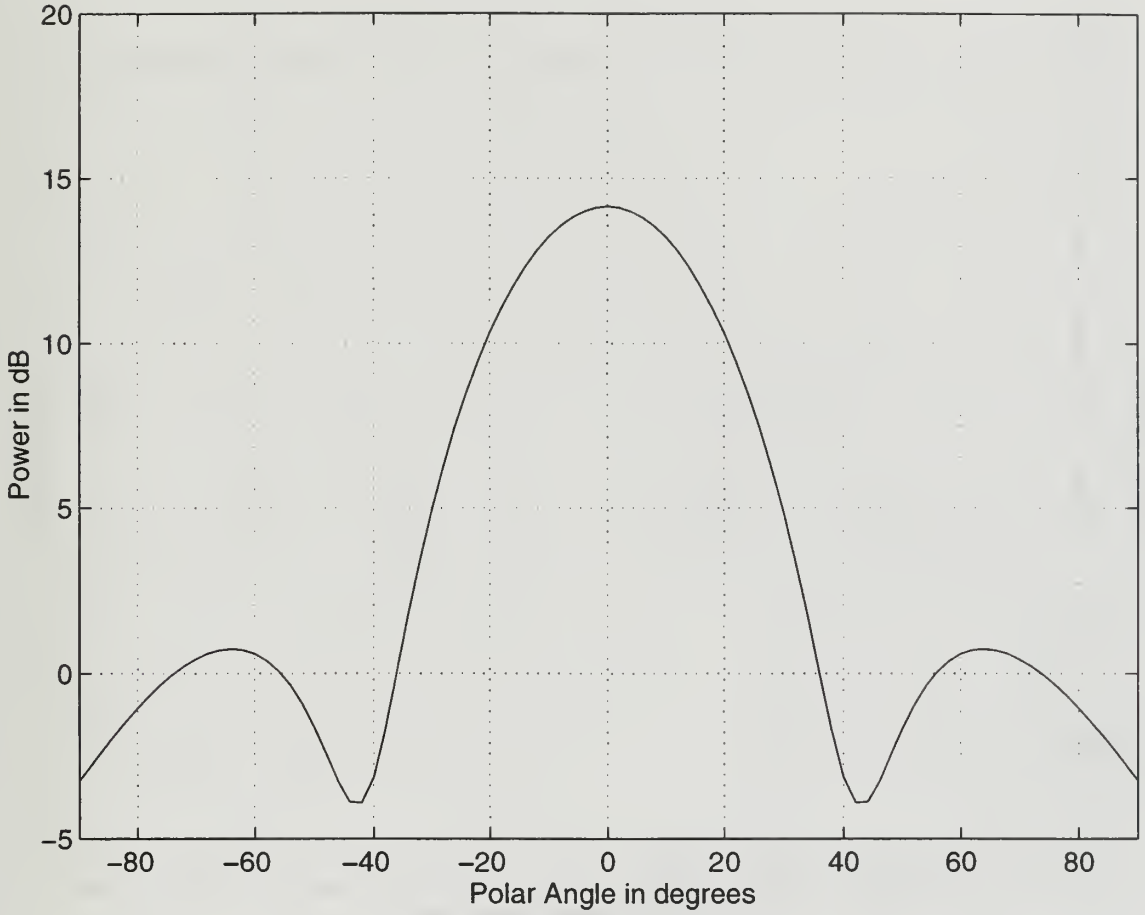

Figure 15. Radiation pattern for three elements over a finite ground plane ($\phi = 0^{o}$).

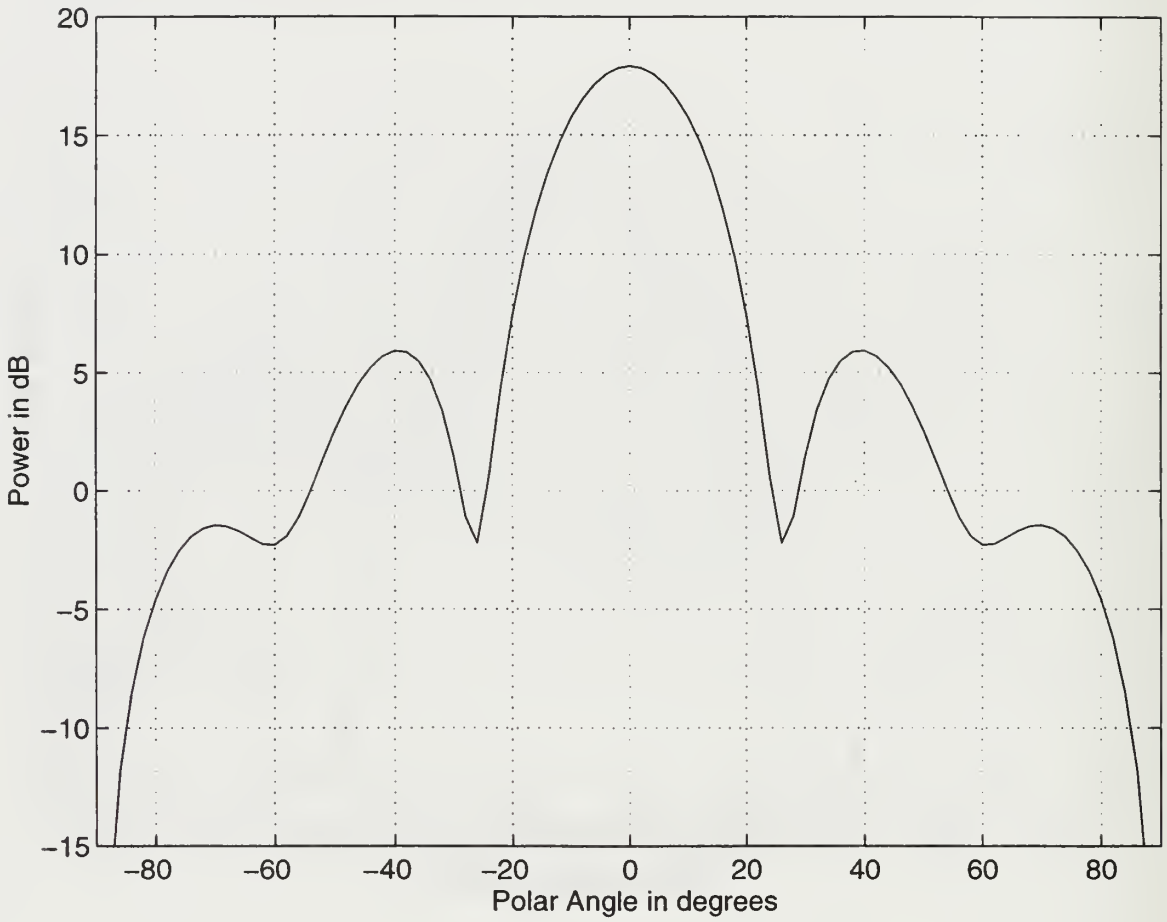

Figure 16. Radiation pattern for five elements over an infinite ground plane ($\phi = 0^{o}$).

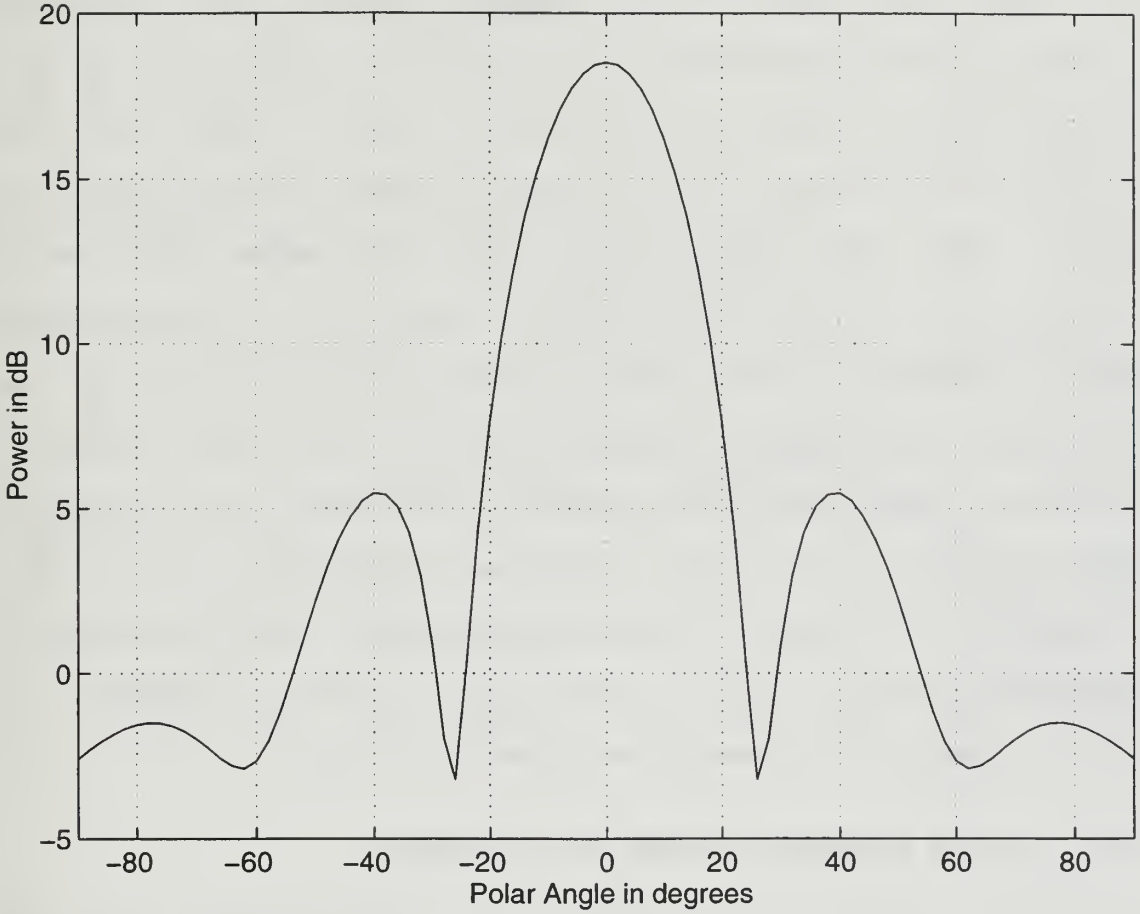

Figure 17. Radiation pattern for five elements over a finite ground plane ($\phi = 0^o$).

previously mentioned, the radiation resistance for a single isolated dipole is 73 Ohms. Using the computed value of the current across the edge that corresponds to the feed point of the dipole, and dividing by the impressed voltage, the driving point impedance is obtained. For an array with an infinite ground plane the resistance is 73 Ohms only for the middle dipole, while the outer two have a value of 40.26 Ohms. For an array with a finite ground plane, values of 72.96 and 40.66 Ohms occur at the center and edges respectively. When the array is increased to five dipoles over a infinite ground plane, the resulting values of the radiation resistance are 43.83 Ohms for the middle element, 68.98 Ohms for the first elements on either side of center and 40.72 Ohms for the outermost elements. For a five element array above a finite ground plane the resistance of the middle dipole is 42.1 Ohms, the adjacent elements are 75.13 Ohms and the outer ones are 39.35 Ohms.

B. ACTIVE ELEMENT PATTERN AND SCANNING

It is useful to note the contribution of each individual element to the shape of the array radiation pattern. In order to do so, we compute the pattern with only one element excited and all other elements loaded. These are referred to as active element patterns. Figure 18 shows the element factors of each dipole for infinite and finite

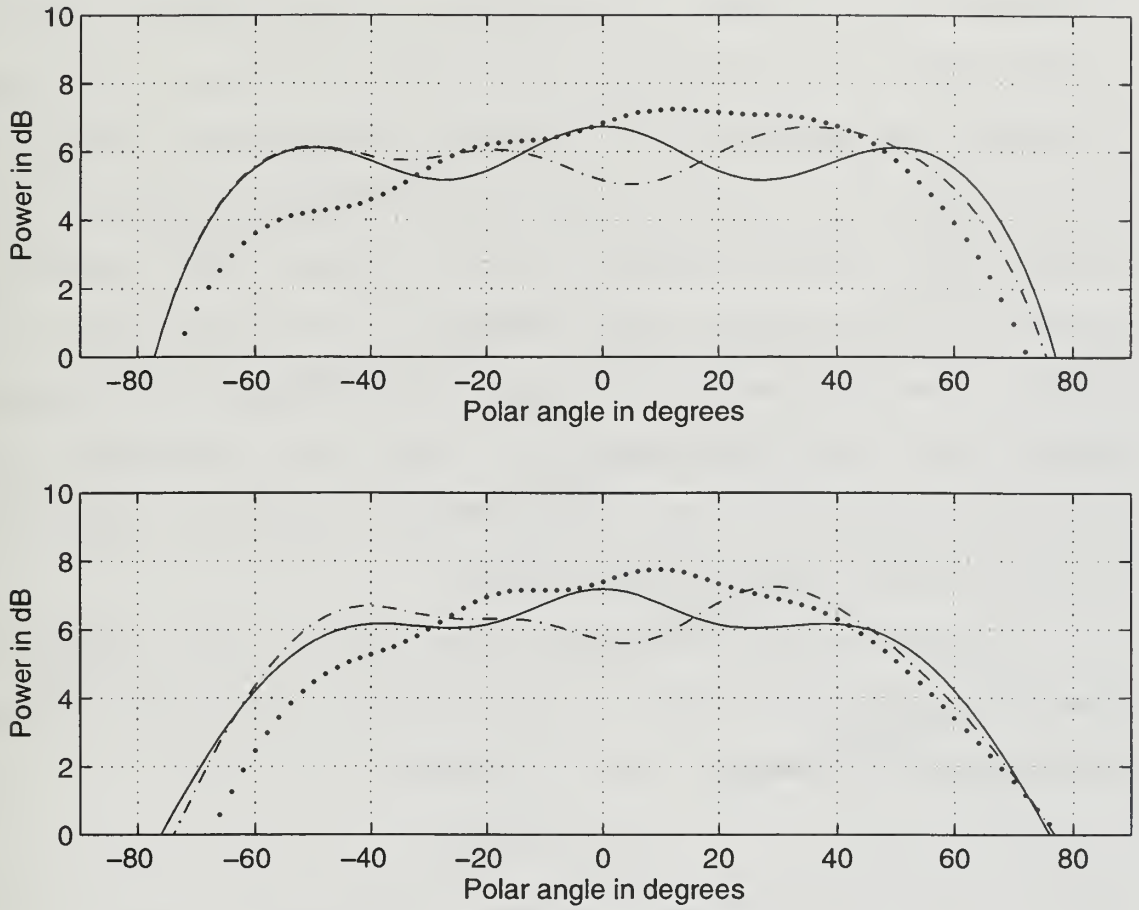

Figure 18. Top: element factors for five elements over an infinite ground plane as in Figure 19. Bottom: element factors for five elements over a finite ground plane as in Figure 7. Solid line: element 3, dash-dotted line: element 2, dotted line: element 1 ($\phi = 0^{o}$ for all plots).

ground planes. In each case the excited dipole is labeled and all of the rest of the elements are loaded with a resistance of 50 Ohms. The pattern of the center element (solid line) is symmetrical in θ. The patterns of the edge elements are asymmetrical. Element patterns for dipoles 4 and 5 will be mirror images of 2 and 1 (Figure 19), respectively, and therefore are not plotted. For the array with the finite ground plane (Figure 7) the element patterns tend to be narrower than those for the infinite ground plane. That is, the directivity drops more quickly as a function of angle. This implies that the array gain will decrease more rapidly with scanning.

To examine the gain loss with scan we can steer the beam to a specific angle by introducing a successive phase shift between elements given by formula

$$\Delta\phi = kd\sin(\theta_s)$$

where d is the distance between the elements and θ_s the desired steering angle. For the given d and $\theta_s = -25^o$ the necessary phase shift is calculated to be 60.85 degrees per element. The results for infinite and finite ground planes are shown in Figure 20.

The element spacing in an array is used as a design parameter for matching, that is obtaining a resonance in the radiation impedance. To illustrate, if the distance between the elements decreases from 0.4λ to 0.35λ then the pattern

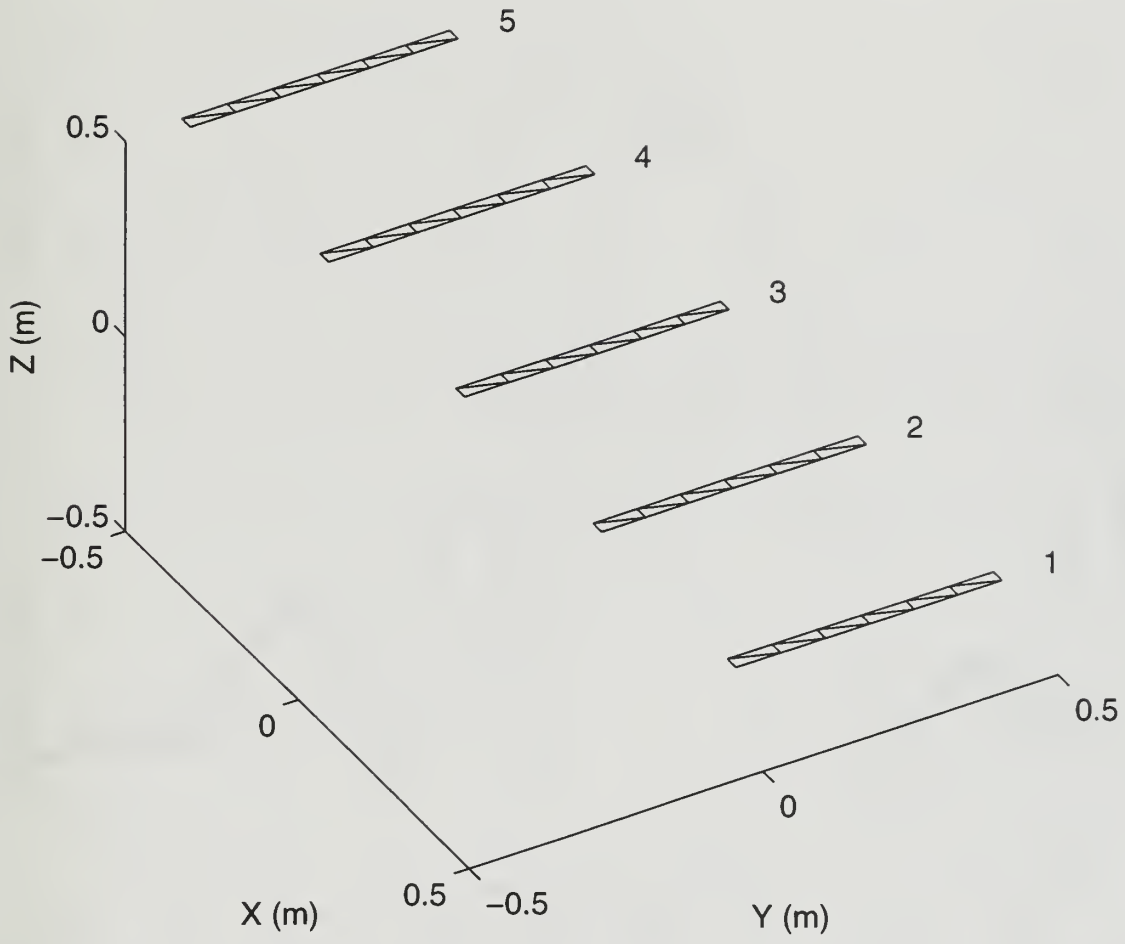

Figure 19. Five elements over an infinite ground plane.

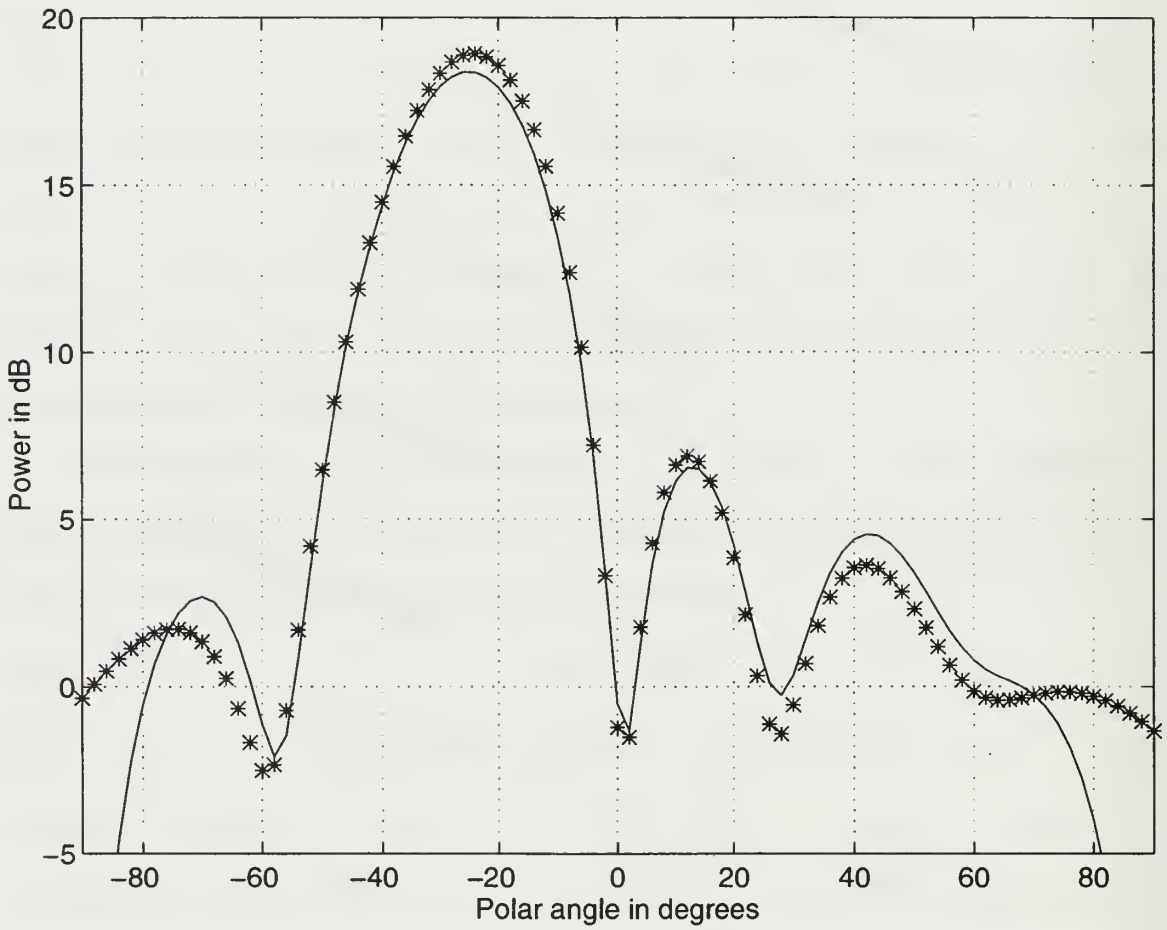

Figure 20. Radiation pattern for five elements with the beam steered to -25 degrees. Solid line: over infinite ground plane; crosses: over finite ground plane ($\phi = 0^o$).

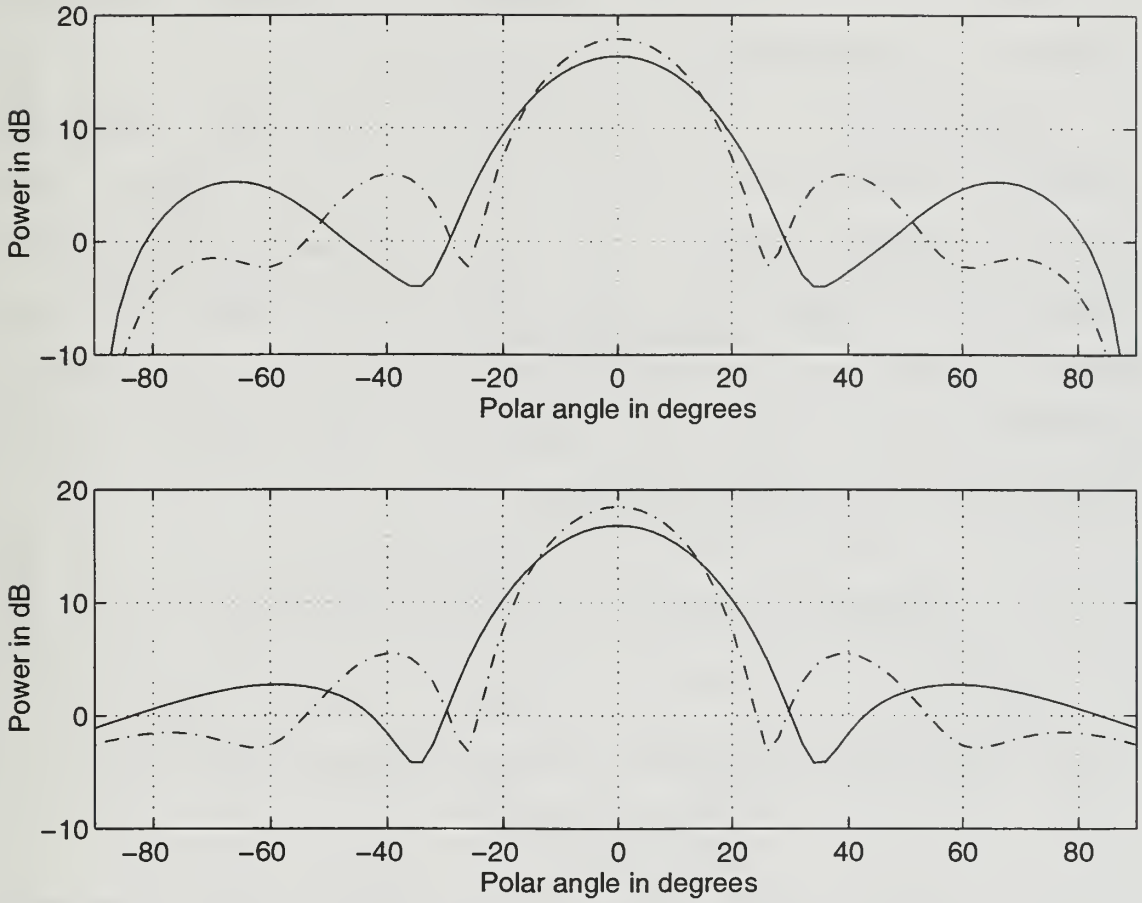

Figure 21. Radiation pattern for five elements when the distance between the elements is $d = 0.35\lambda$ (solid line) in comparison with the original geometry where $d = 0.4\lambda$ (Dash-dotted line). Top: infinite ground plane. Bottom: finite ground plane ($\phi = 0^o$).

in Figure 21 is obtained. A modification of the ground plane is needed in order to maintain the edge distances of 0.5 wavelength beyond the outermost element. The new dimensions are 2.625 by 1.45 wavelength. As we can see, the decrease in the spacing moves the first sidelobe to a wider angle and increases the beamwidth.

Additionally, the directivity has been reduced, primarily because the array area has been reduced. The active element patterns for the reduced spacing are displayed in Figure 22 for infinite and finite ground planes. There are no significant changes in the element paterns due to the new spacing. The driving point impendances are given in Table 1.

Spacing in λ	Ground plane	Element position		
		(3)	(2)	(1)
d=0.4	finite	42.1	75.13	39.35
	infinite	43.83	68.98	40.72
d=0.35	finite	19.67	35.96	32.65
	infinite	20.67	37.33	33.35

Table 1. Driving point impedances as a function of spacing. Entries are the magnitudes.

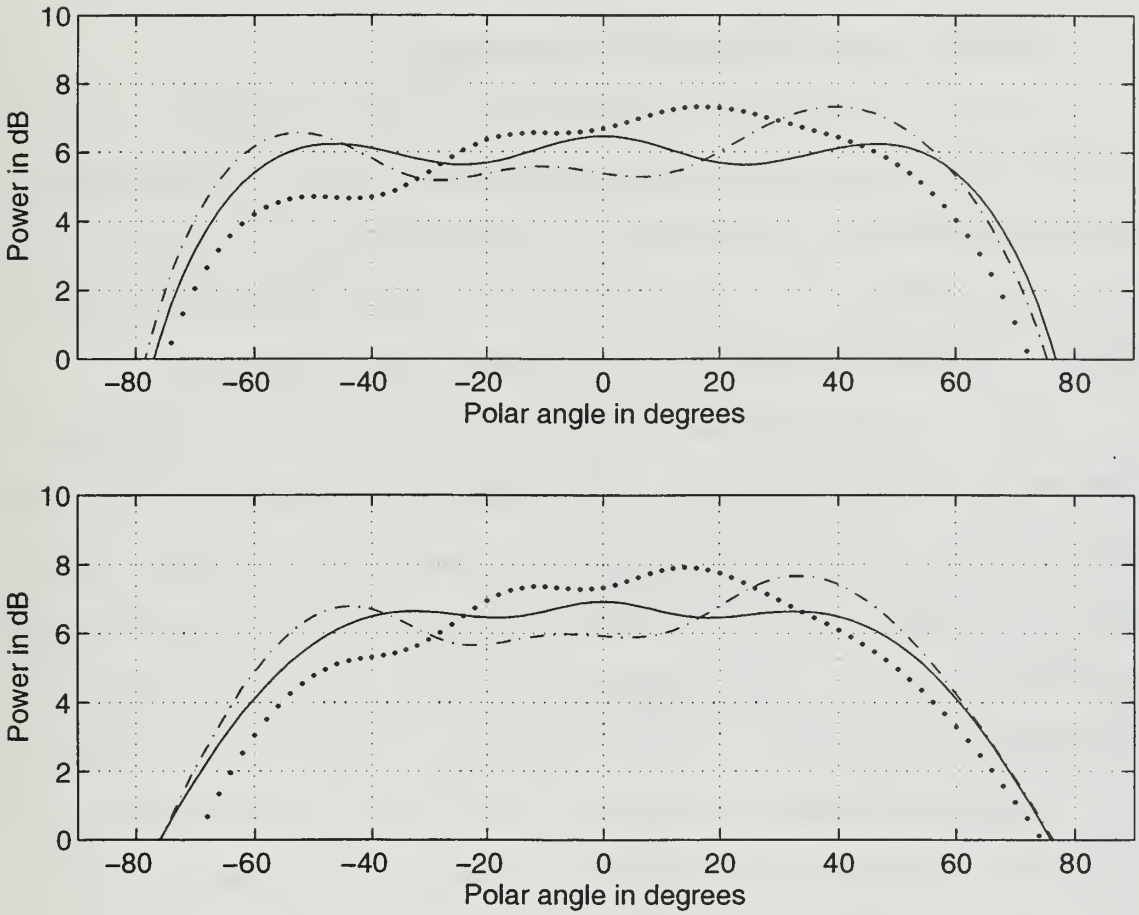

Figure 22. Top: element factors for five elements over an infinite ground plane as in Figure 19. Bottom: element factors for five elements over a finite ground plane as in Figure 7. Solid line: element 3, dash-dotted line: element 2, dotted line: element 1. The distance between the elements is 0.35 wavelength ($\phi = 0^o$).

Finally, patterns are computed for the main beam scanned to -25^{o}. The radiation patterns for the infinite and finite ground planes are presented in Figure 23.

C. GROUND PLANE SHAPES AND SIDELOBES

So far a number of radiation patterns for a linear, five-element array have been presented. All of the patterns have an increase in wide-angle sidelobes due to ground plane edge scattering. In an effort to reduce this scattering, several different ground plane shapes were examined.

For a rectangular ground plane, the maximum edge scattering occurs in the $x-z$ and $y-z$ planes, which are transverse to the plate edges. By changing the edge angle, the direction of the scattering maximum can be changed. This approach may not be acceptable since the scattering is redirected elsewhere, simply moving the lobe, not reducing it. A more effective treatment is to use a serrated edge or "zig zag" which would spread the scattered energy over a wide range of angles. In order to investigate the impact of the ground plane edges, the pattern is computed for triangle heights of 0.5 and 1.5 wavelengths (Figures 24 and 25 respectively). Figure 26 shows the principal plane patterns for the two different triangular edge profiles as well as the straight edge. It is quite obvious that we can obtain a significant decrease in the principal plane sidelobe level for angles greater than 80 degrees. Specifically, there is a

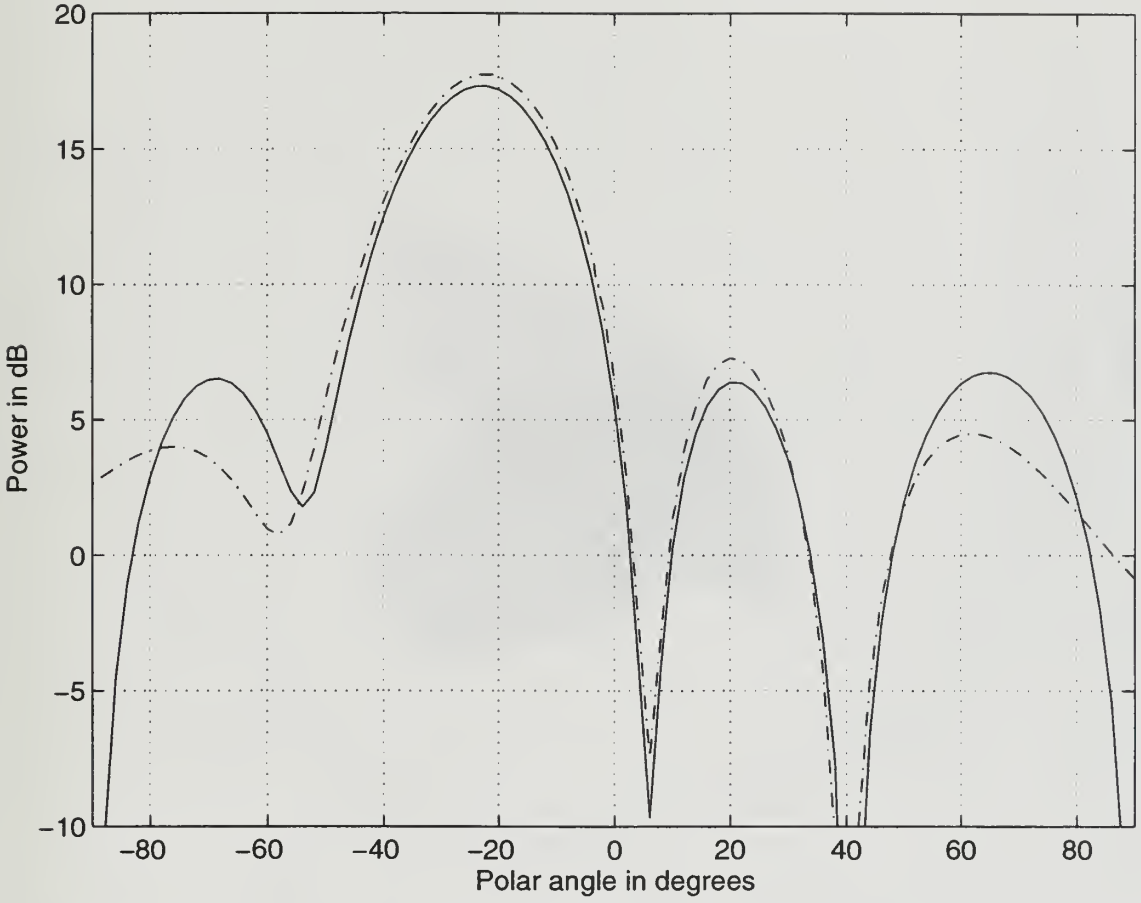

Figure 23. Radiation patterns for five elements (d=0.35 wavelength) and the beam steered to -25 degrees. Solid line: over an infinite ground plane; Dash-dotted line: over a finite ground plane ($\phi = 0^{o}$).

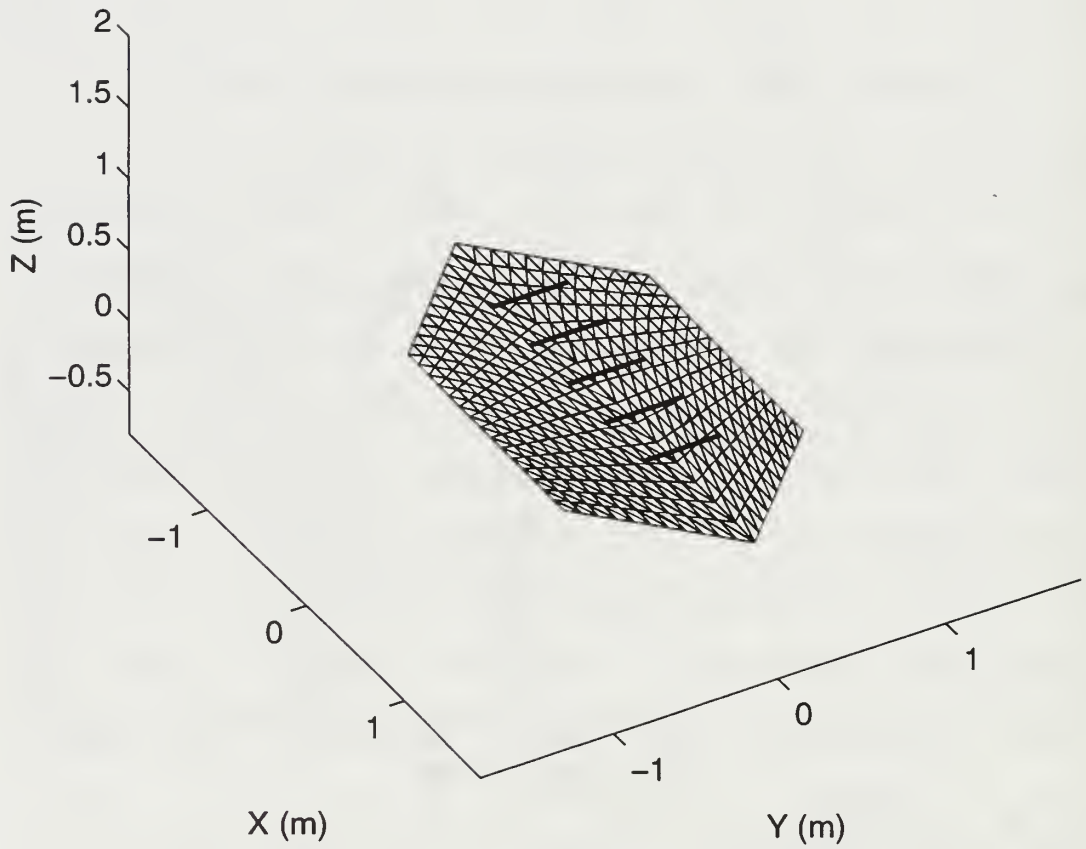

Figure 24. Shaped ground plane with triangular edges of height 0.5 wavelength.

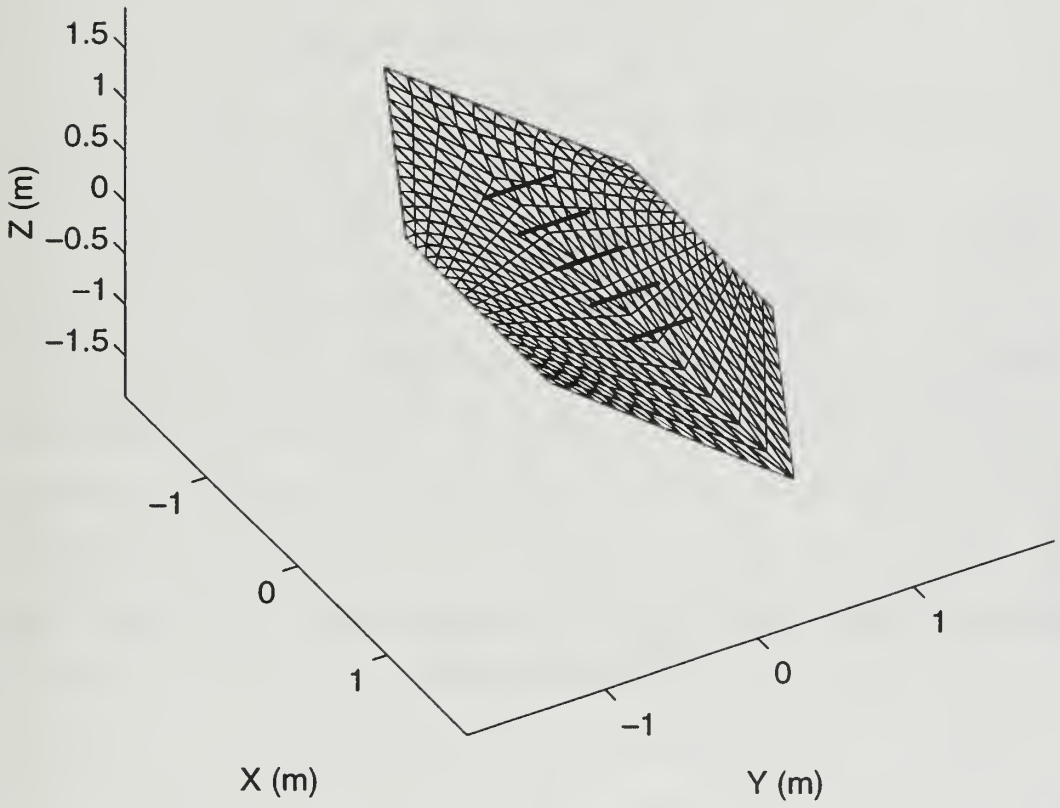

Figure 25. Shaped ground plane with triangular edges of height 1.5 wavelength.

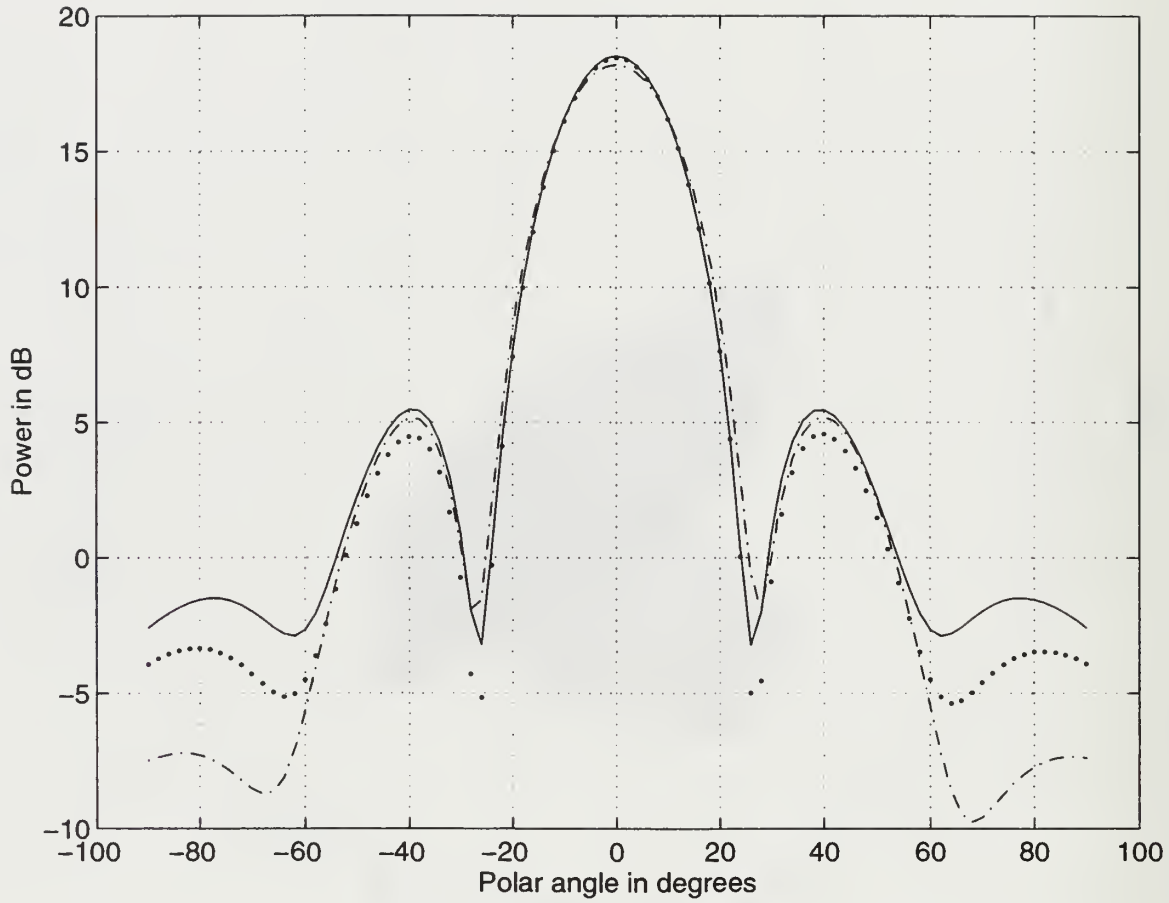

Figure 26. Radiation pattern for the geometry of Figure 7 (solid line), Figure 24 (dotted line) and Figure 25 (dashed-dotted line), ($\phi = 0^o$).

decrease of more than five dB from the original case. The energy is being scattered out of the principal plane and it is expected that the sidelobe levels will be increased in the ϕ plane perpendicular to the slanted edge. For this reason we examine the radiation patterns in direction cosine space as they are shown in Figures 27 through 29 for the straight and slanted ground plane edges. Pattern cuts for $\phi = 20$ and 45 degrees are shown in Figure 30. The sidelobes for a scanned beam at $\theta = -25$ degrees are evident in the contour plots in Figures 31 through 33.

Another ground plane property that might affect the pattern is the extent beyond the edges of the dipole in the $x-z$ plane. Previously the ground plane edge extended 0.5 wavelength beyond the dipole. Three new geometries are created as shown in Figures 34 through 36 where the distance between the edge of the ground plane and those of the dipoles is 0.1 wavelength. The pattern plots for each geometry are shown in Figure 37. A significant change only occurs for case when the ground plane has a triangle edge with height of 0.5 wavelength, where the modified geometry shows a significant loss in gain relative to the larger ground plane. More complete view of the radiation calculations is provided in Figures 38 through 40.

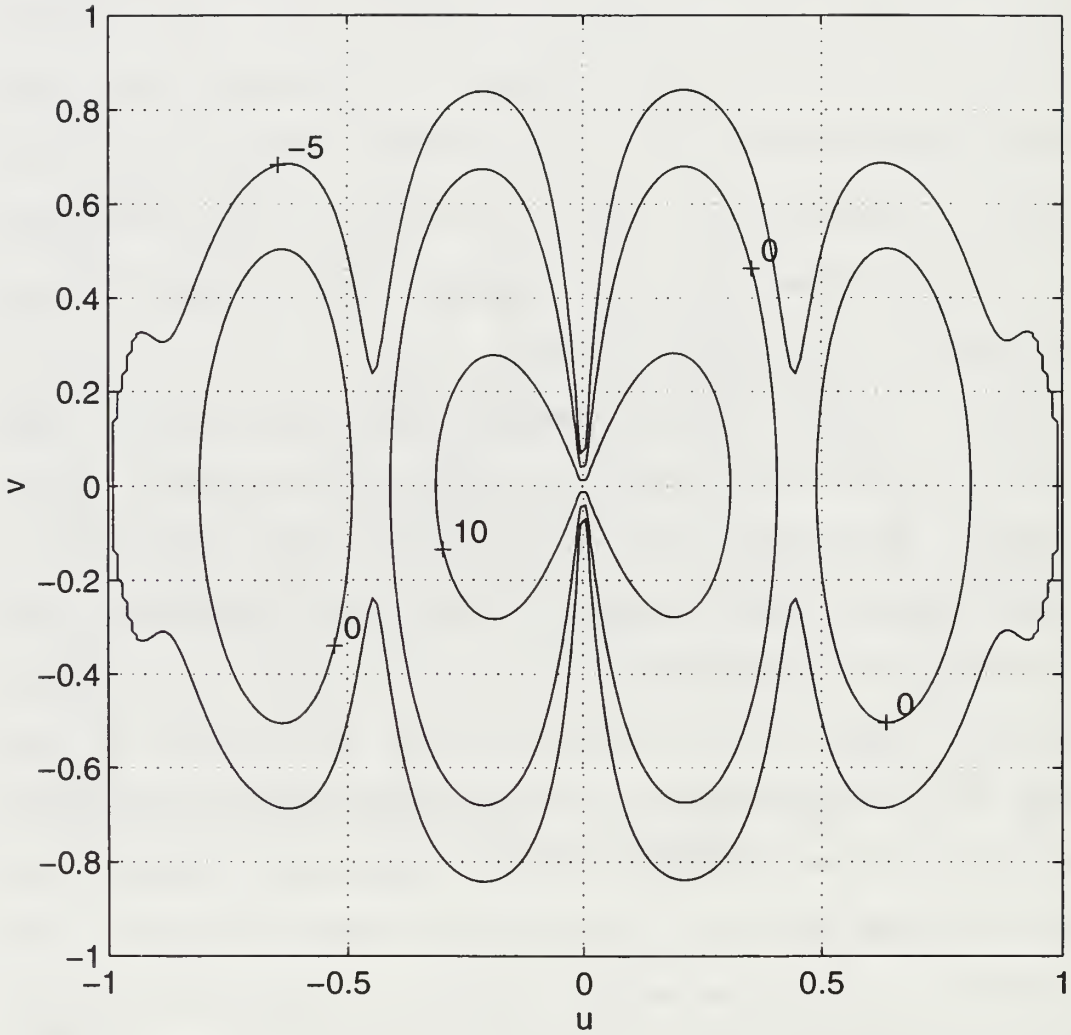

Figure 27. Radiation pattern in direction cosine space (contour plot in dB) for the geometry of Figure 7.

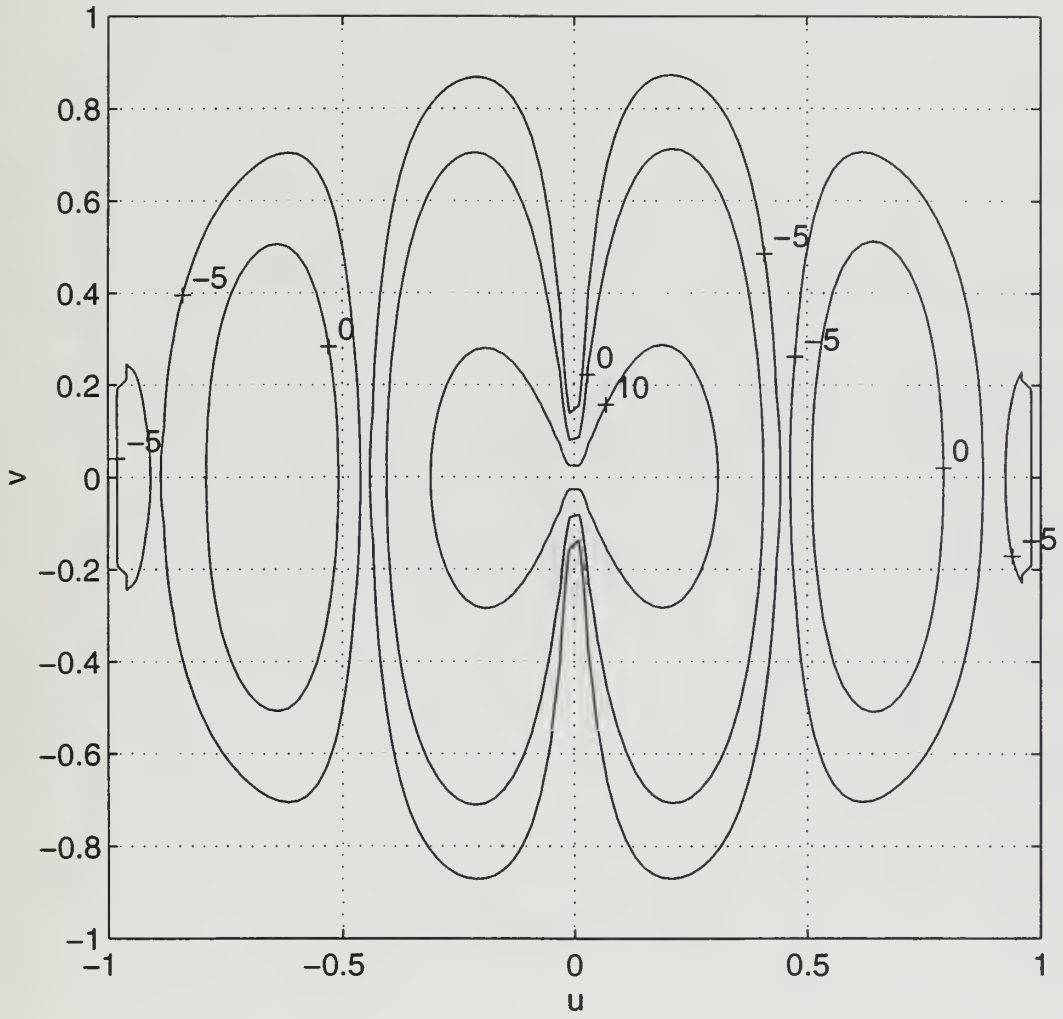

Figure 28. Radiation pattern in direction cosine space (contour plot in dB) for the geometry of Figure 24.

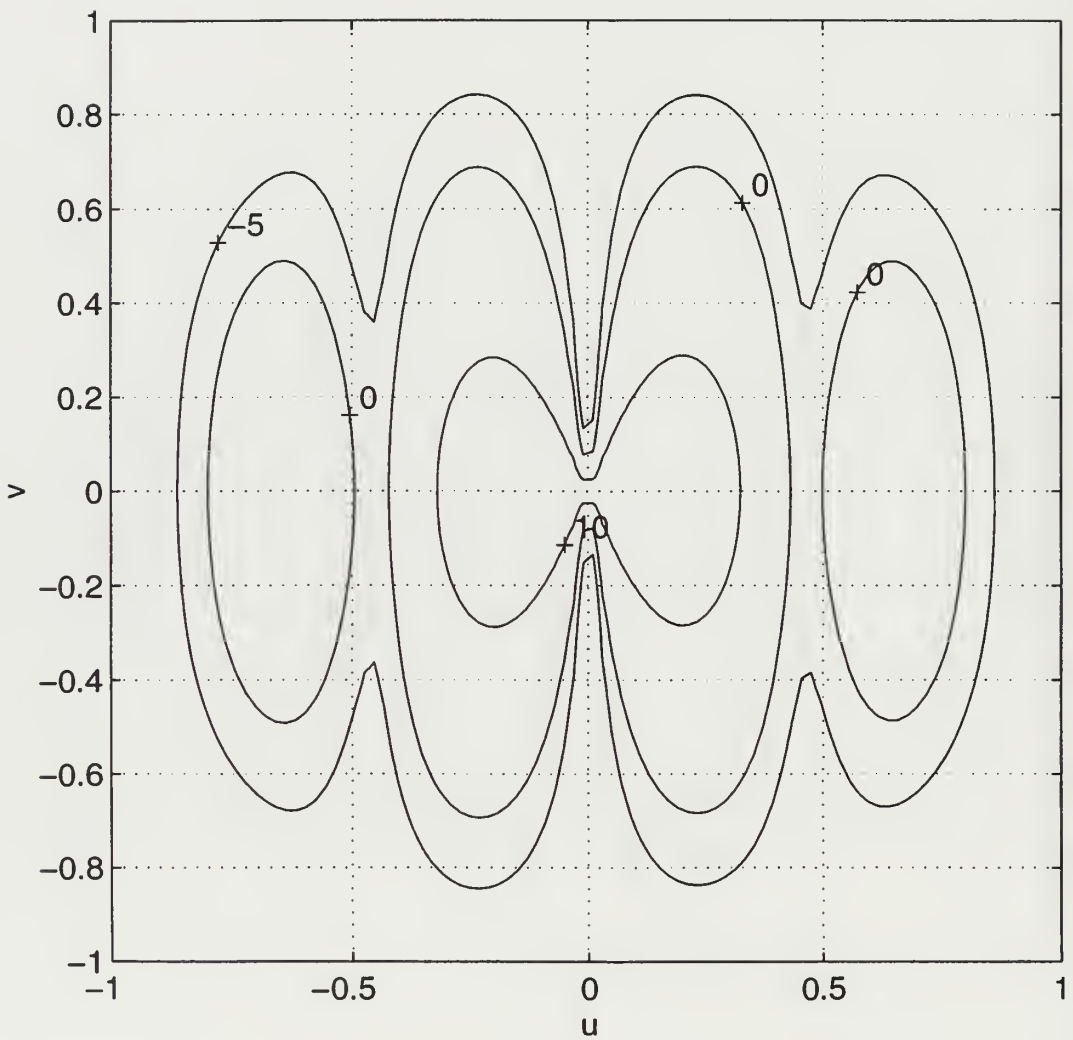

Figure 29. Radiation pattern in direction cosine space (contour plot in dB) for the geometry of Figure 25.

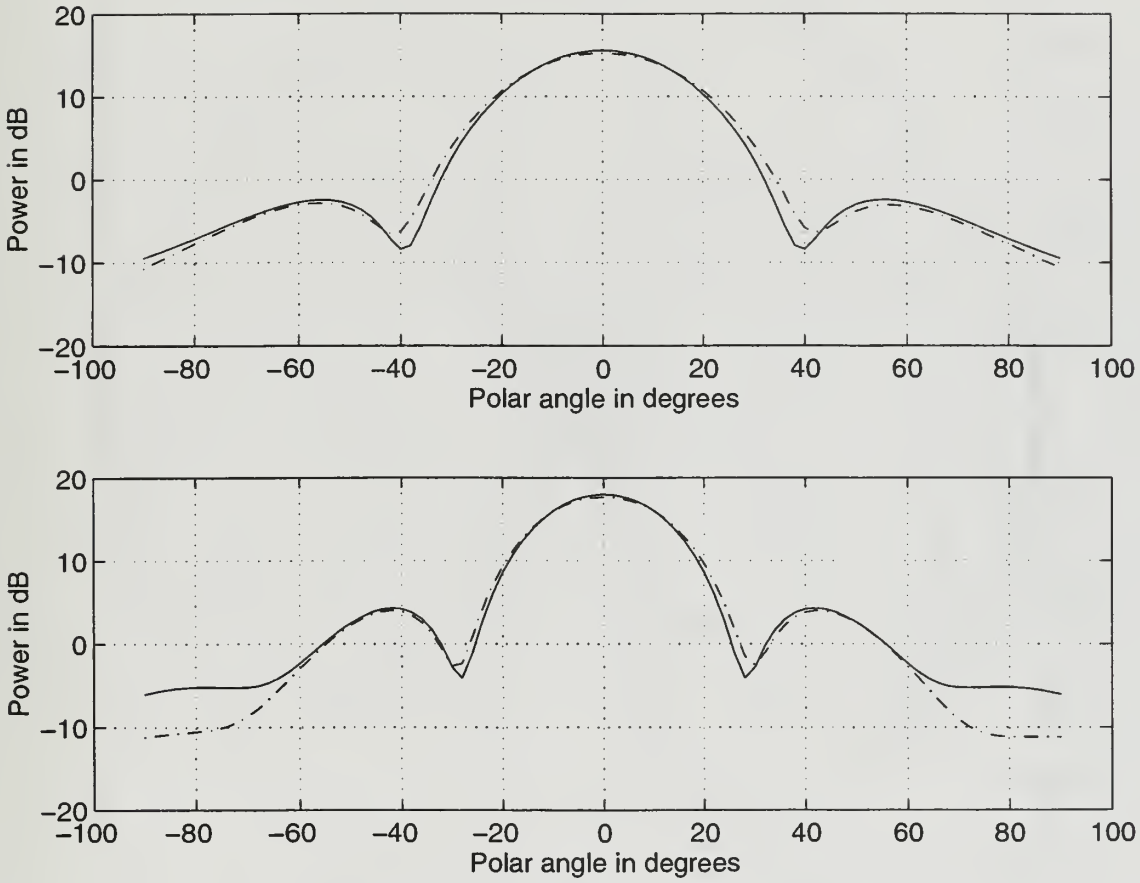

Figure 30. Top: radiation pattern cut at $\phi = 45^{o}$. Bottom: radiation pattern cut for $\phi = 20^{o}$. Solid line: geometry of Figure 7; dotted line: geometry of Figure 25.

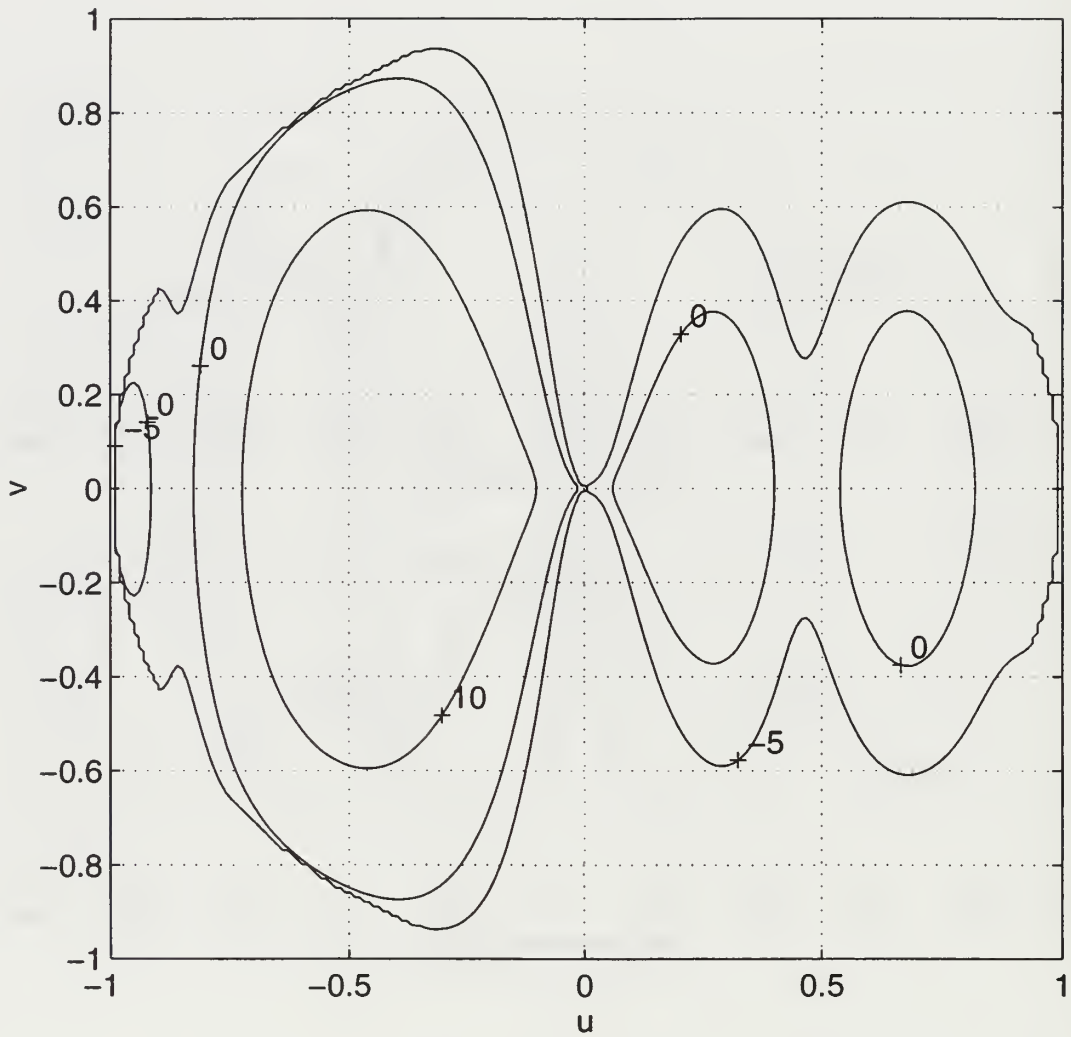

Figure 31. Contour plot (in dB) in direction cosine space for the beam steered to $\theta = -25^{o}$ for the geometry of Figure 7.

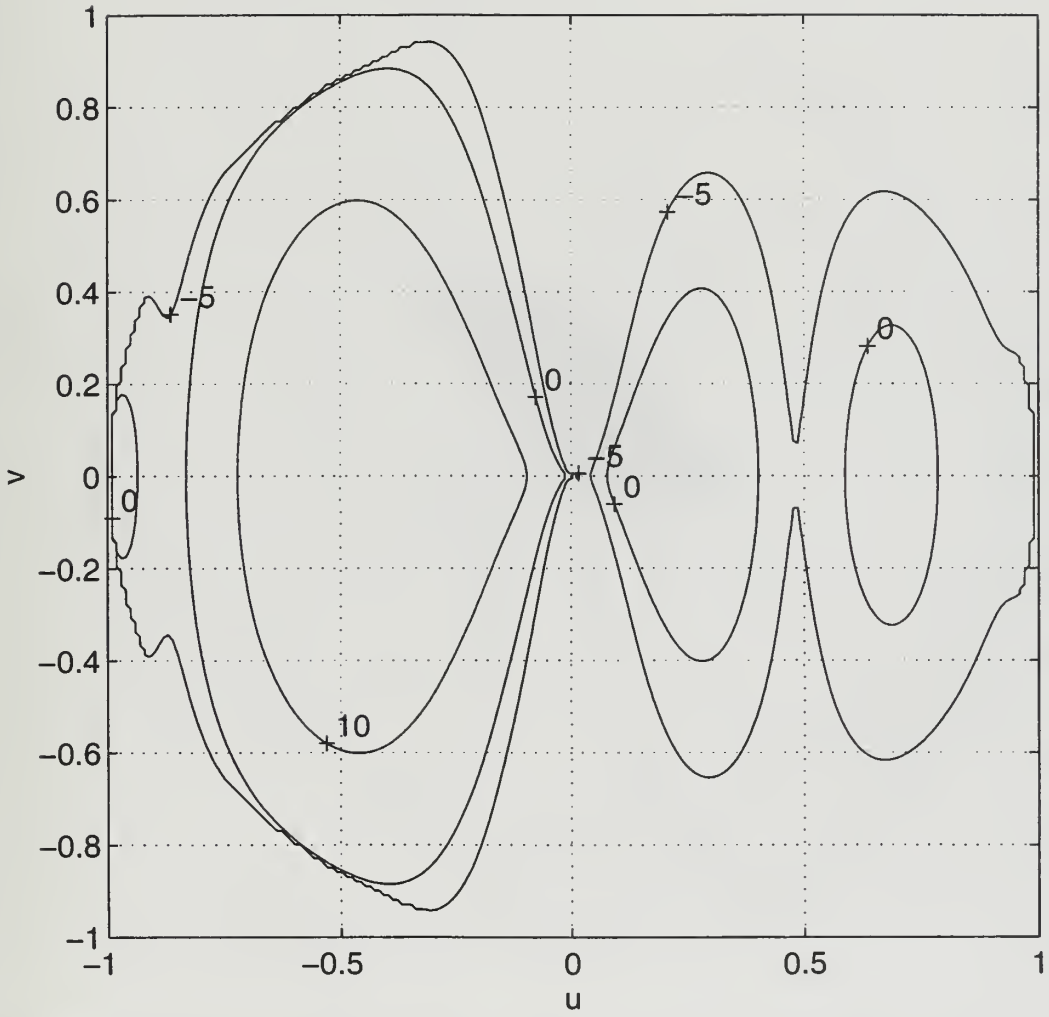

Figure 32. Contour plot (in dB) in direction cosine space for beam steered to $\theta = -25^{o}$ for the geometry of Figure 24.

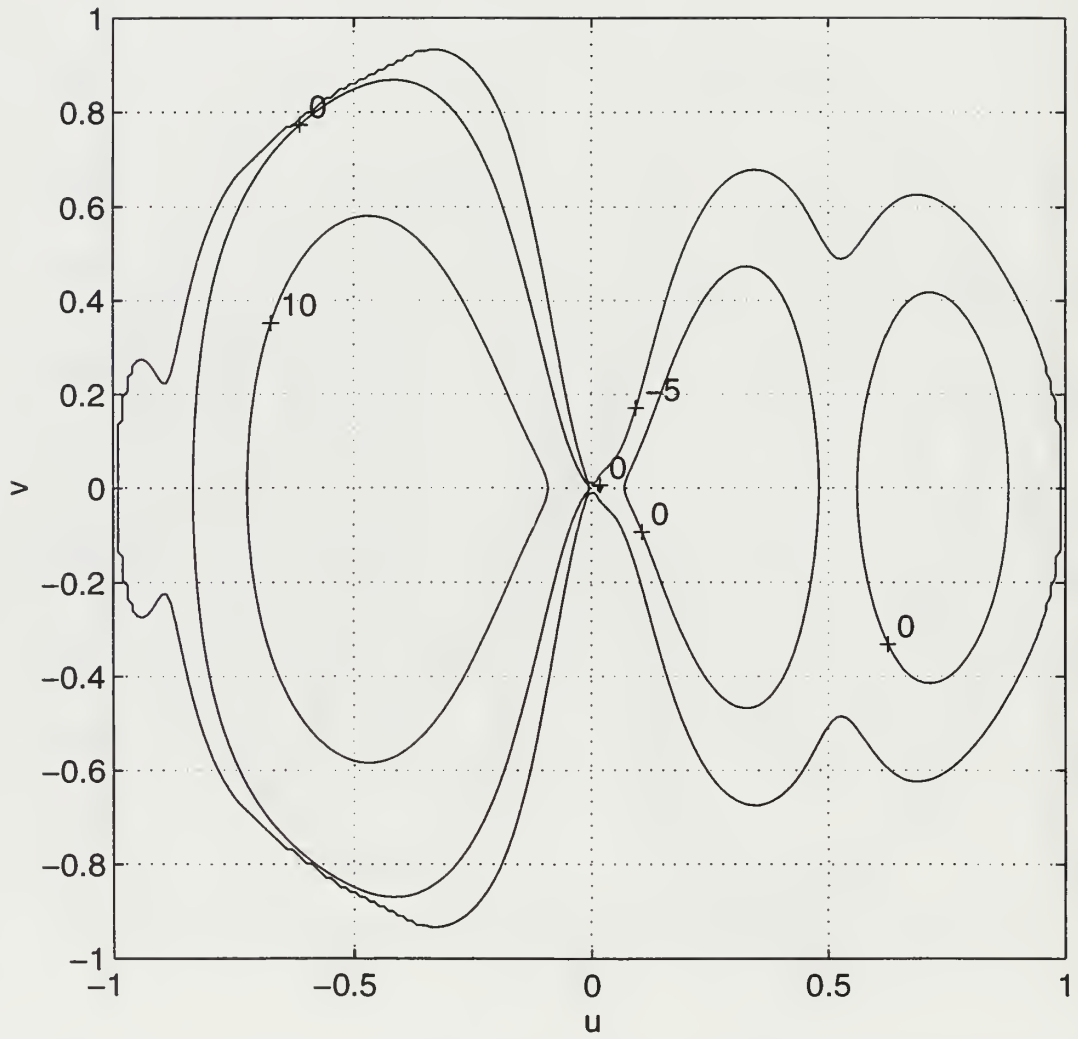

Figure 33. Contour plot (in dB) in direction cosine space for the beam pattern steered at $\theta = -25^{o}$ for the geometry of Figure 25.

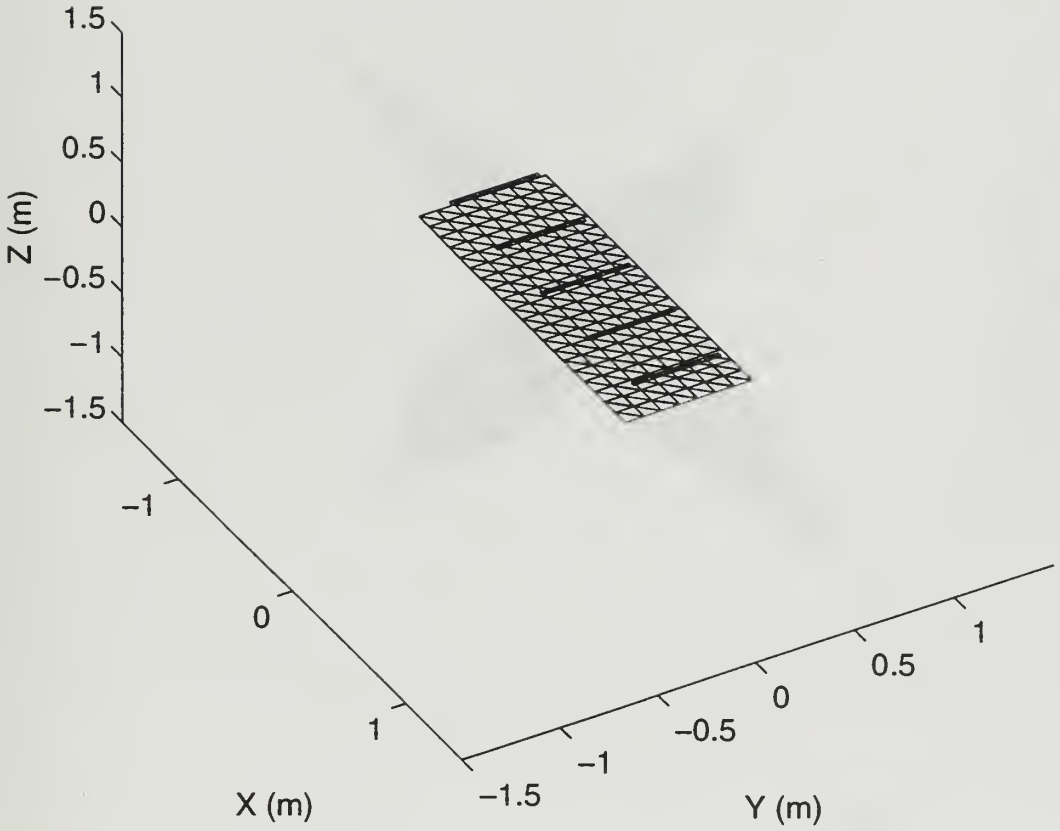

Figure 34. Five elements over a finite ground plane with reduced dimensions (0.65 by 1.05 wavelengths).

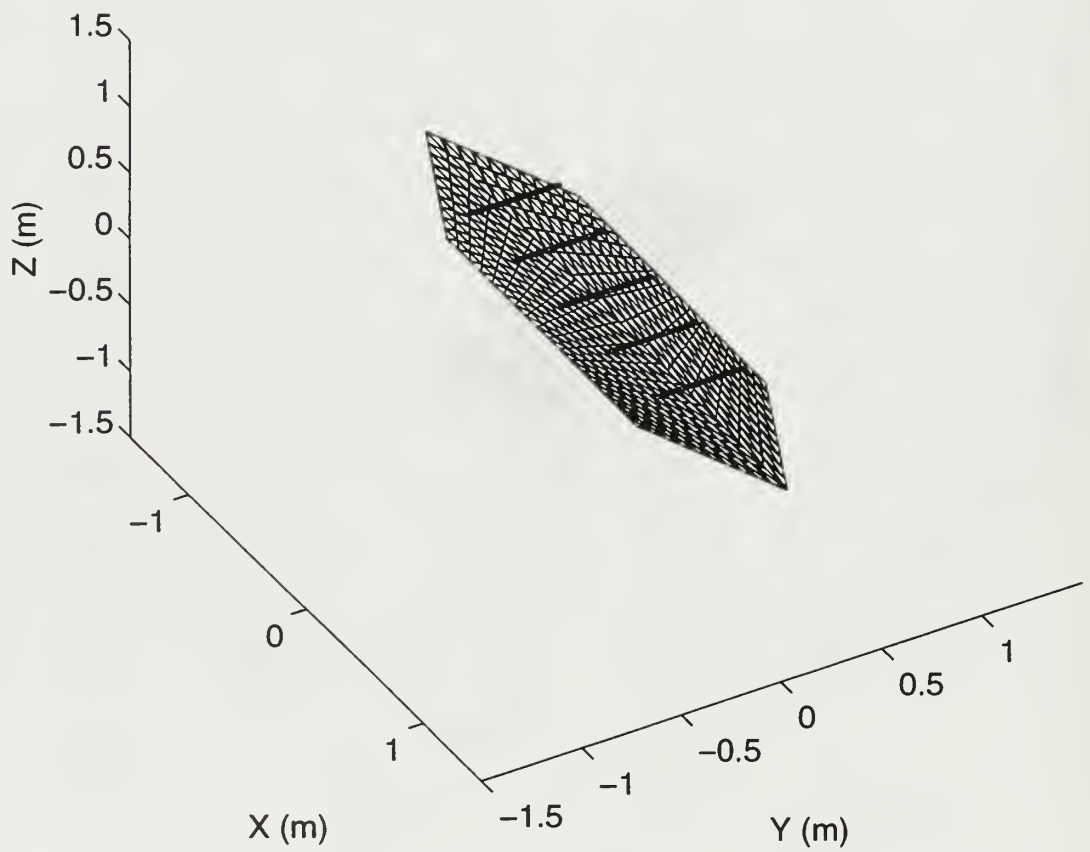

Figure 35. Geometry similar to Figure 24 with the ground plane edges extending 0.1 wavelength beyond the dipole edge.

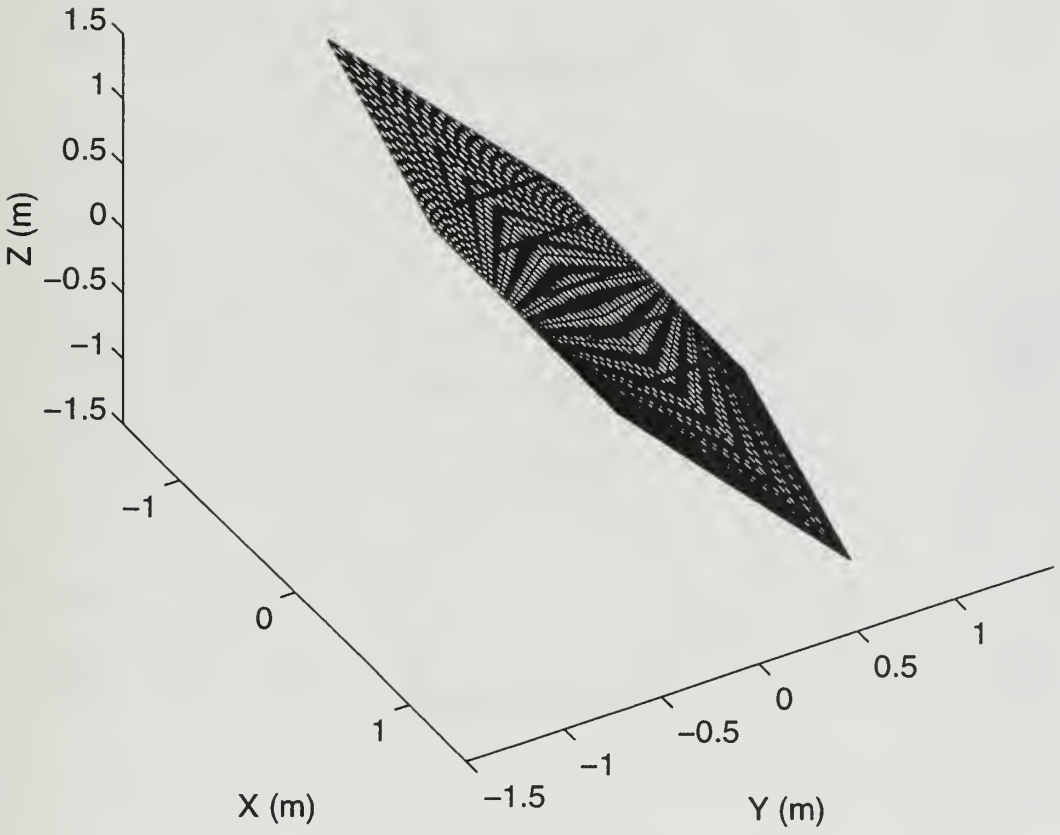

Figure 36. Geometry similar to Figure 25 with the ground plane edges extending 0.1 wavelength beyond the dipole edge.

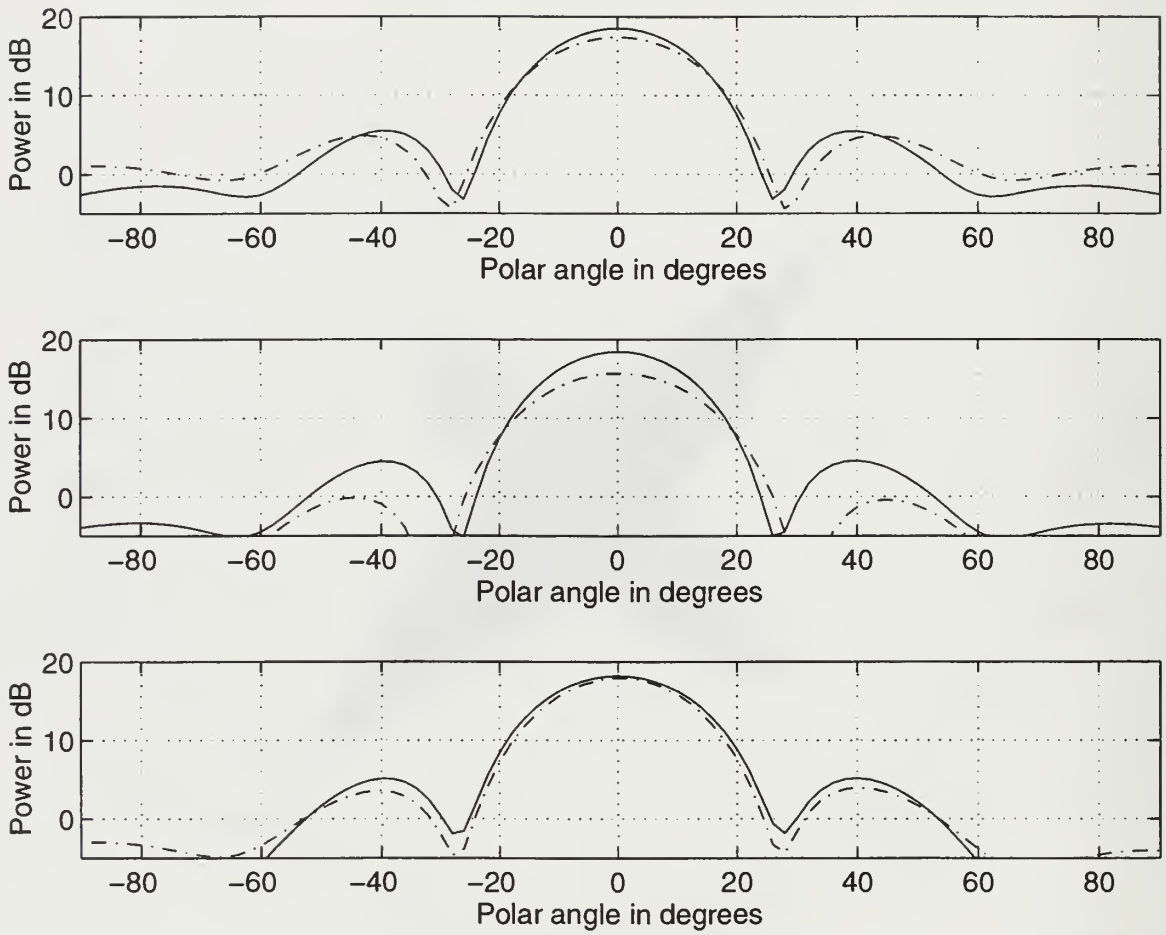

Figure 37. Top: ground plane with straight edges, center: ground plane with triangular edges (triangle height of 0.5 wavelength). Bottom: ground plane with triangular edges (triangle height of 1 wavelength). Solid line: edge extents 0.5 wavelength. Dash-dotted line: edge extents 0.1 wavelength ($\phi = 0^o$).

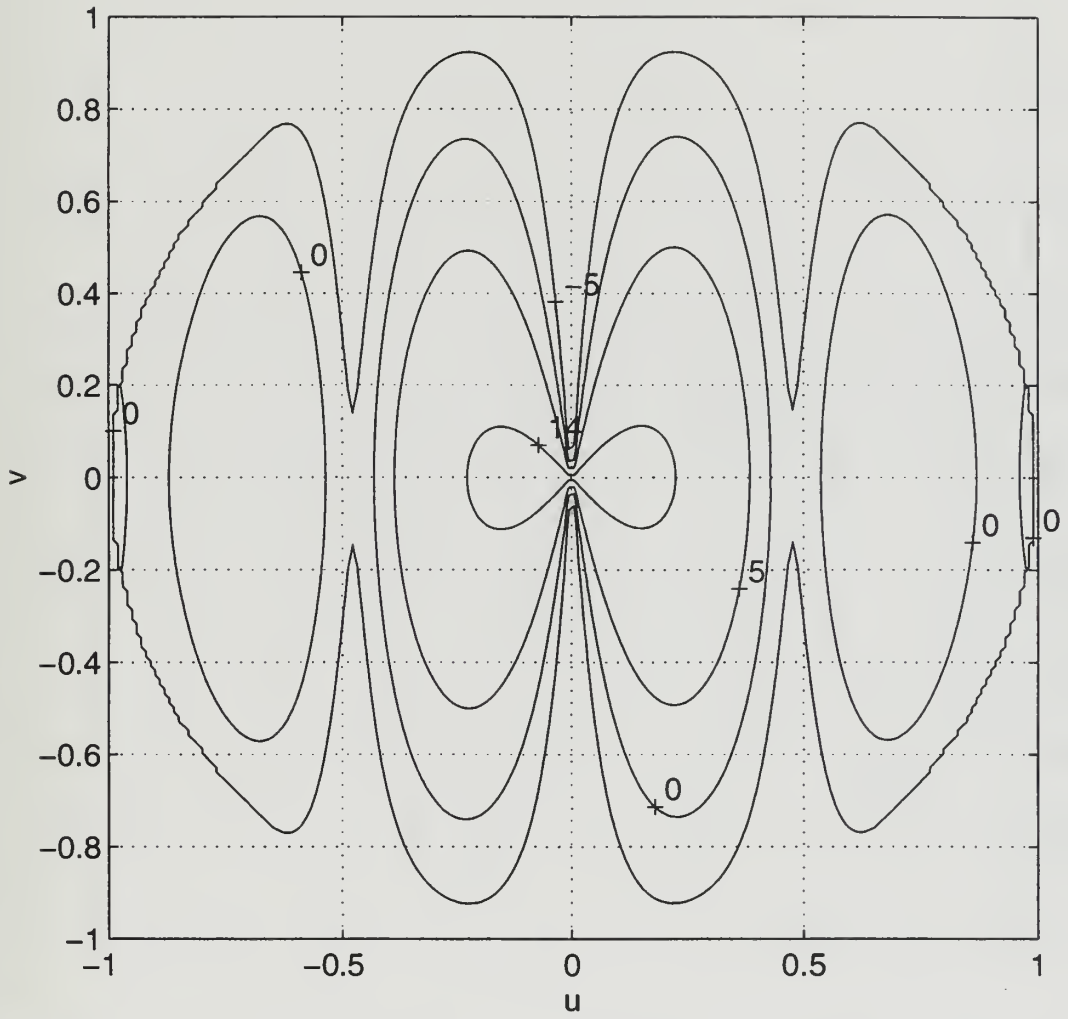

Figure 38. Radiation pattern in direction cosine space (contour plot in dB) for the geometry of Figure 34.

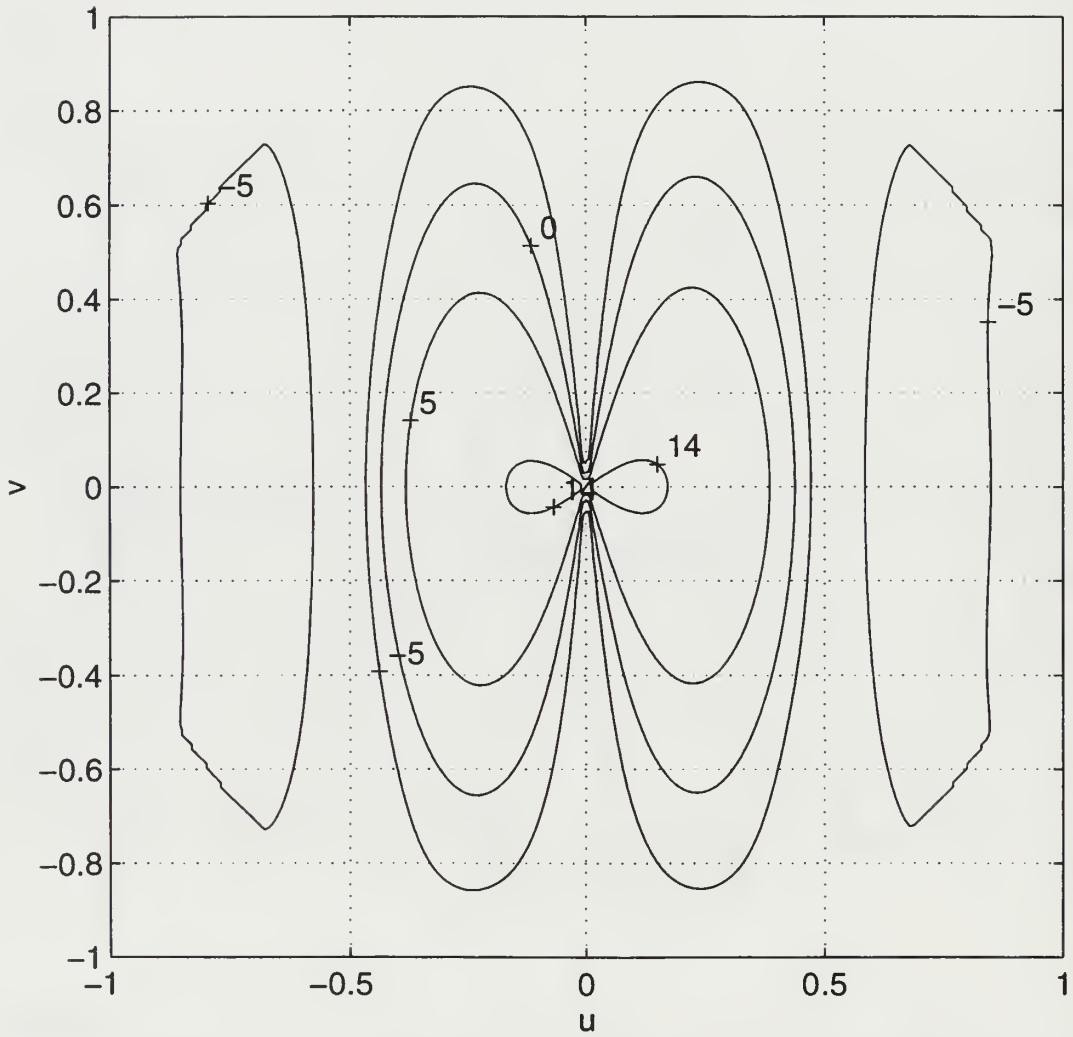

Figure 39. Radiation pattern in direction cosine space (contour plot in dB) for the geometry of Figure 35.

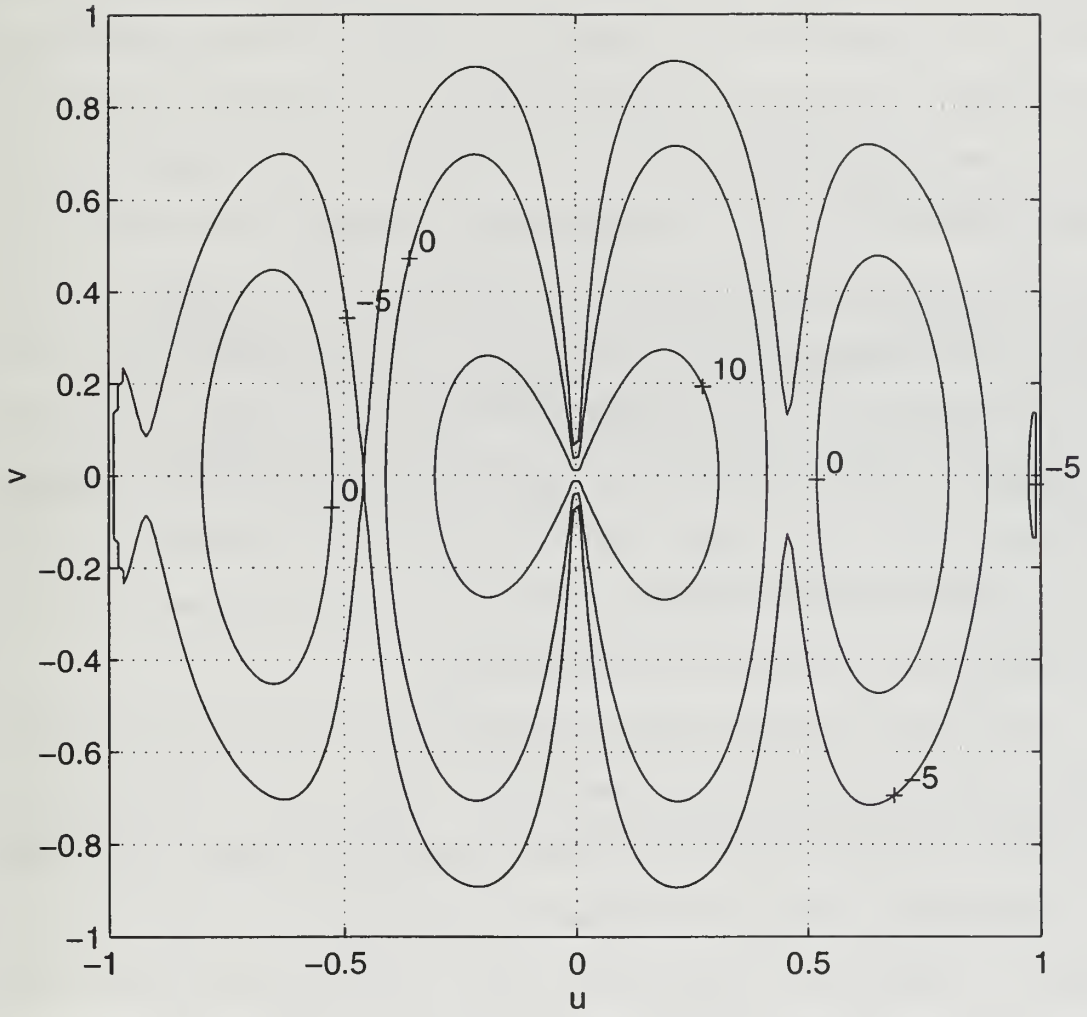

Figure 40. Radiation pattern in direction cosine space (contour plot in dB) for the geometry of Figure 36.

D. CURVED GROUND PLANES

There are many applications where the array aperture must be integrated into a curved surface. Obvious examples include the fuselage and wing of an aircraft. Surfaces are generally classified as singly or doubly curved depending upon whether there is a finite radius of curvature in either one or two principal planes. A cylinder is an example of a singly curved surface; a sphere is a doubly curved surface. A flat geometry can be used to generate a curved one by simply translating the z coordinate of the surface nodes. The procedure is illustrated in Figure 41. Note that when the nodes are translated, the triangle edge lengths increase. Obviously there is a limit to the amount of the translation to be tolerated while still maintaining the 0.1 wavelength restriction for convergence.

The five element array was modified so that the ground plane was cylindrical as shown in Figure 42. The maximum deviation (distance of the curve from a straight line) was 0.1 wavelength. The corresponding pattern for the curved array is shown in Figure 43. For convenience the array factor for an array of 5 elements is also shown. The value for the array factor is given by the formula [Ref. 5]

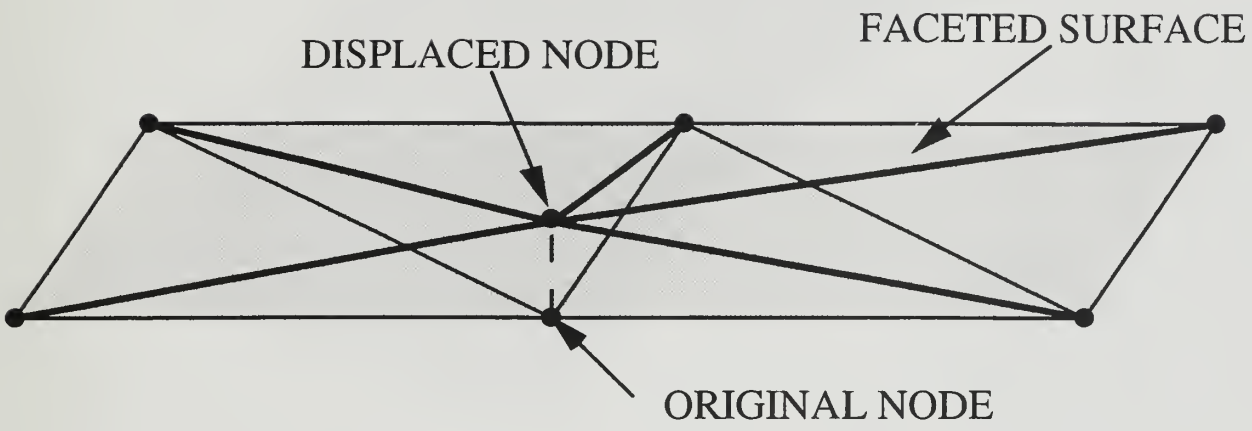

Figure 41. Illustration of patch modification in order to create a curved geometry.

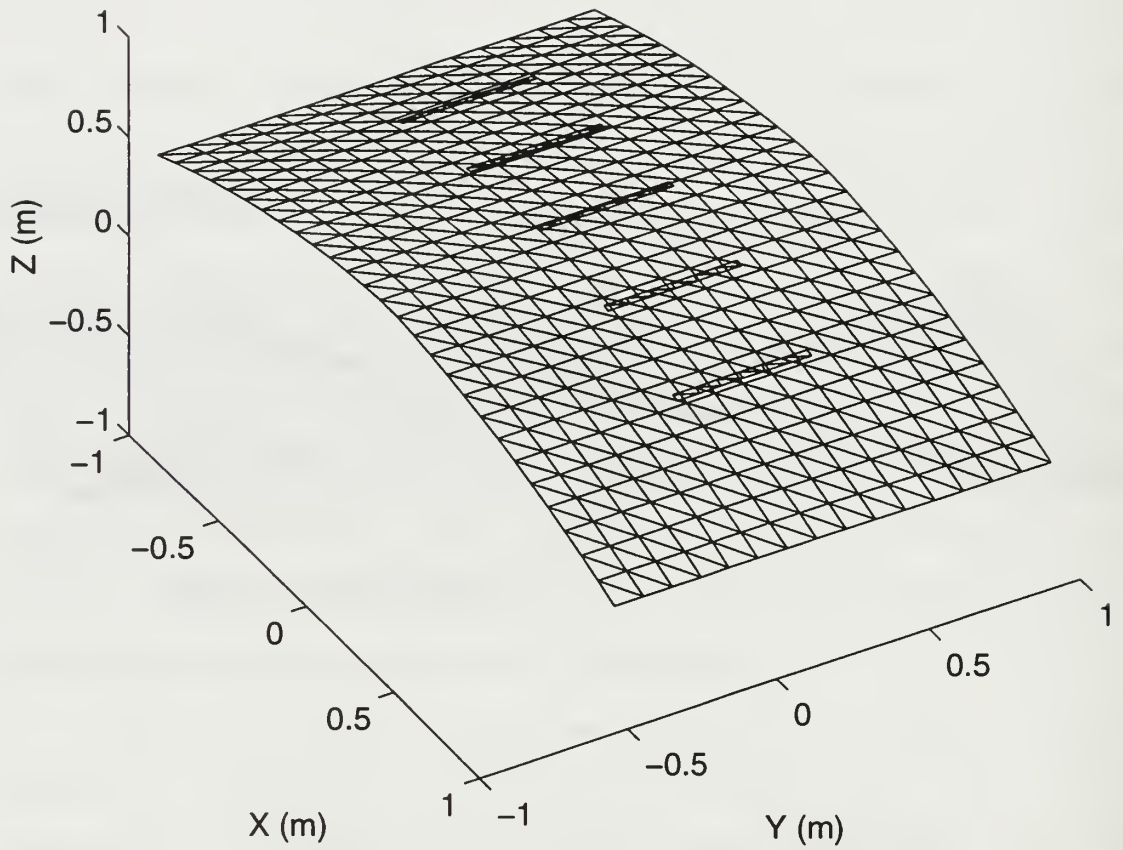

Figure 42. Curved five element array and ground plane.

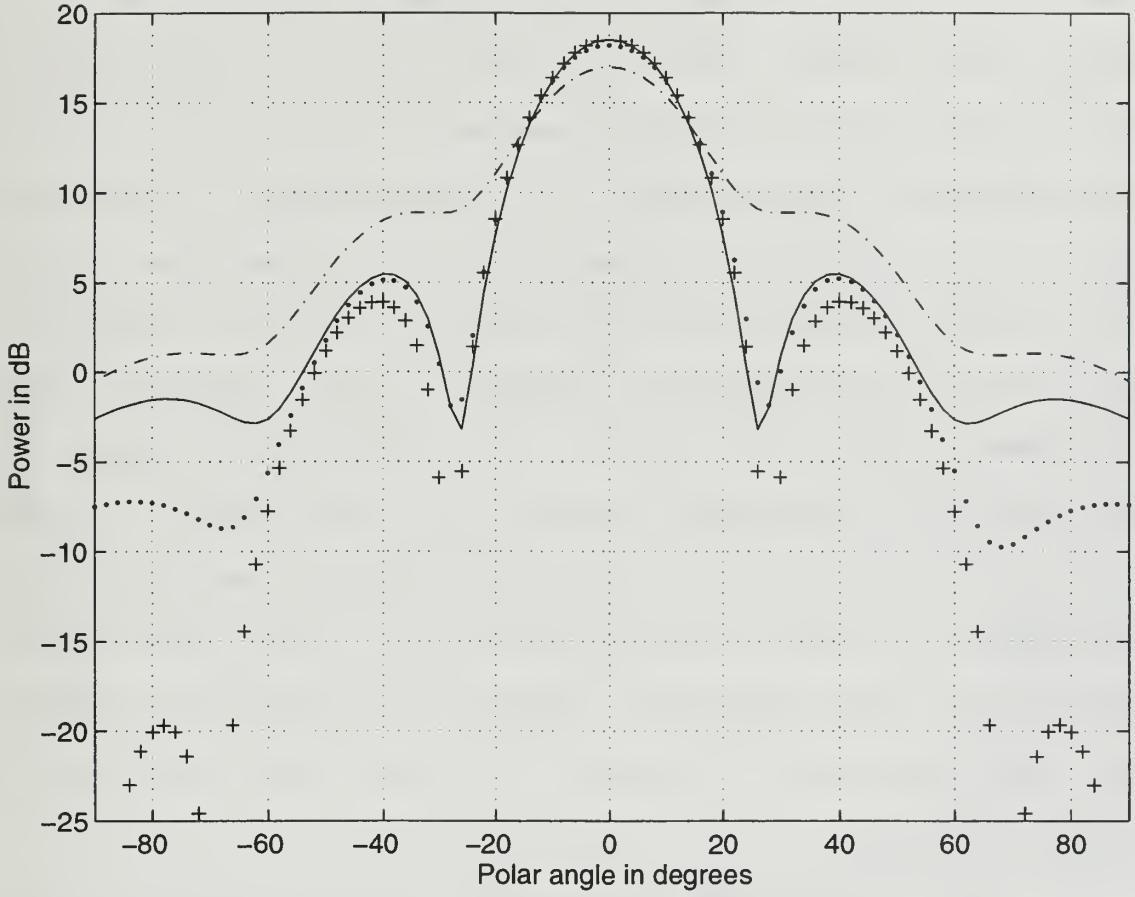

Figure 43. Radiation patterns for the geometries of Figure 42 (dash-dotted line), Figure 7 (solid line), Figure 25 (dotted line) and array factor in Equation 2 (crosses) ($\phi = 0^o$).

$$AF = \frac{\sin\left(\frac{Nkd}{2}\sin(\theta)\right)}{N\sin\left(\frac{kd}{2}\sin(\theta)\right)}\cos(\theta) \qquad (2)$$

where N is the number of the elements and θ the polar angle. For a small array the value of d is not usually equal to the physical spacing because of mutual coupling and edge effects. The distance d is calculated so that the array factor half-power beamwidth has the same value as the one for the original rectangular ground plane. As expected, the directivity has been reduced by the curvature. The displacement of the surface out of a flat plane is equivalent of introducing a phase error. The effects include loss in directivity and increase in the beamwidth and sidelobes. The loss in directivity is 1.7 dB. The element factors for the individual elements are plotted in Figure 44. When the beam is steered to $\theta = -25^{o}$, the patterns in Figure 45 result.

It may be possible to correct for the negative effects of curvature based on the fact that the change in the beam pattern comes from a phase error. The magnitude of this phase error can be calculated from the formula $\Delta\phi = k\Delta z$, where Δz represents the height difference from the flat surface. To compensate for this error we introduce an equal and opposite shift for each element. As shown in Figure 46, the phase error correction results in quite significant

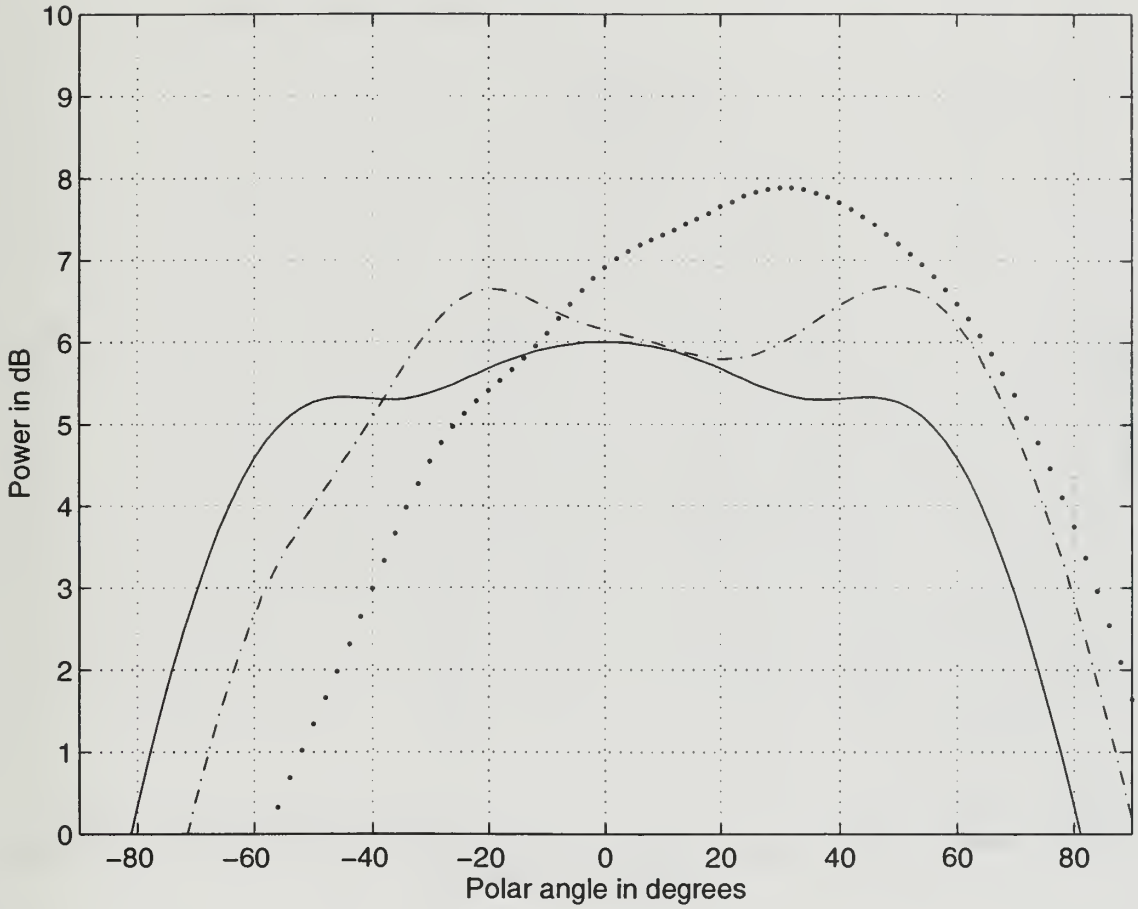

Figure 44. Element factors for a five element array over a finite ground plane as in Figure 42. Solid line: element 3, dash-dotted line: element 2, dotted line: element 1 ($\phi = 0^o$).

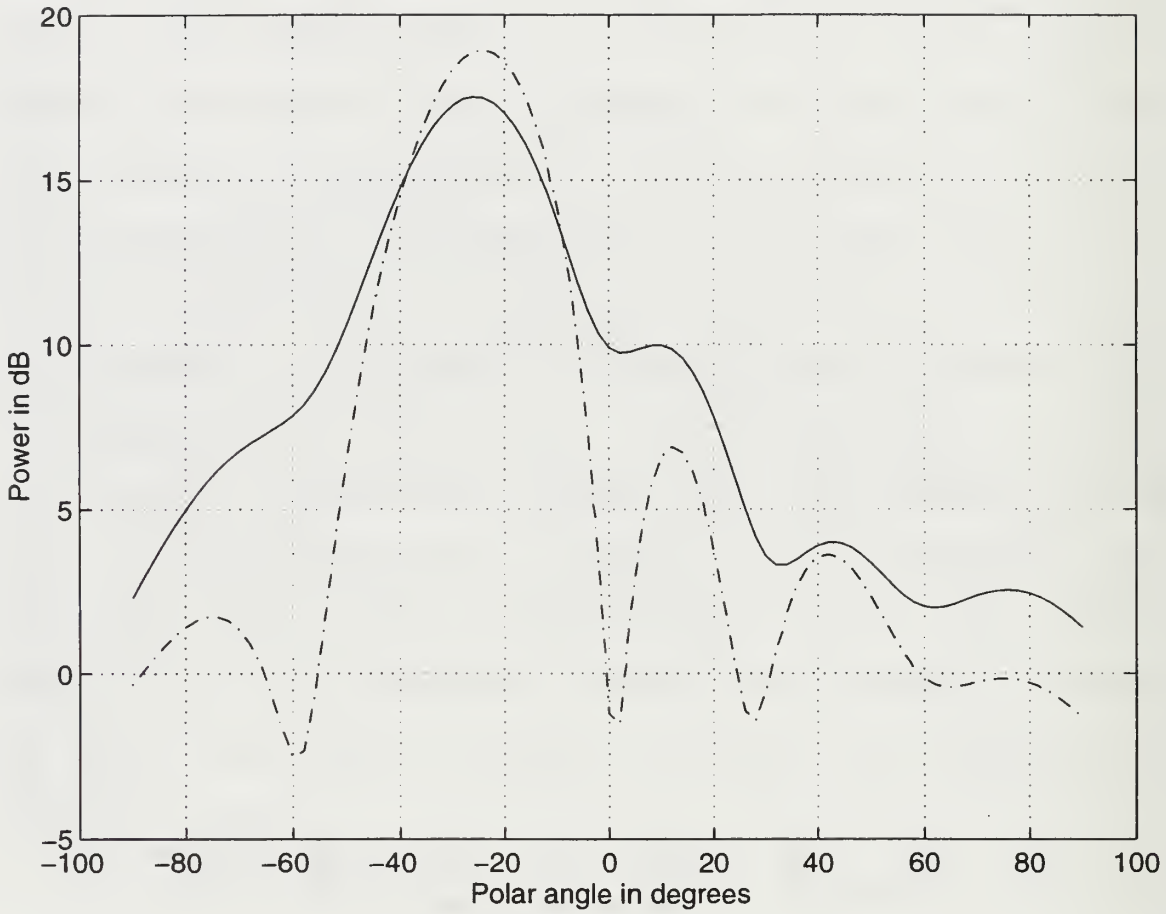

Figure 45. Radiation patterns for the geometries of Figure 42 (solid line) and Figure 7 (dash-dotted line) when the beam is steered to -25 degrees ($\phi = 0^o$).

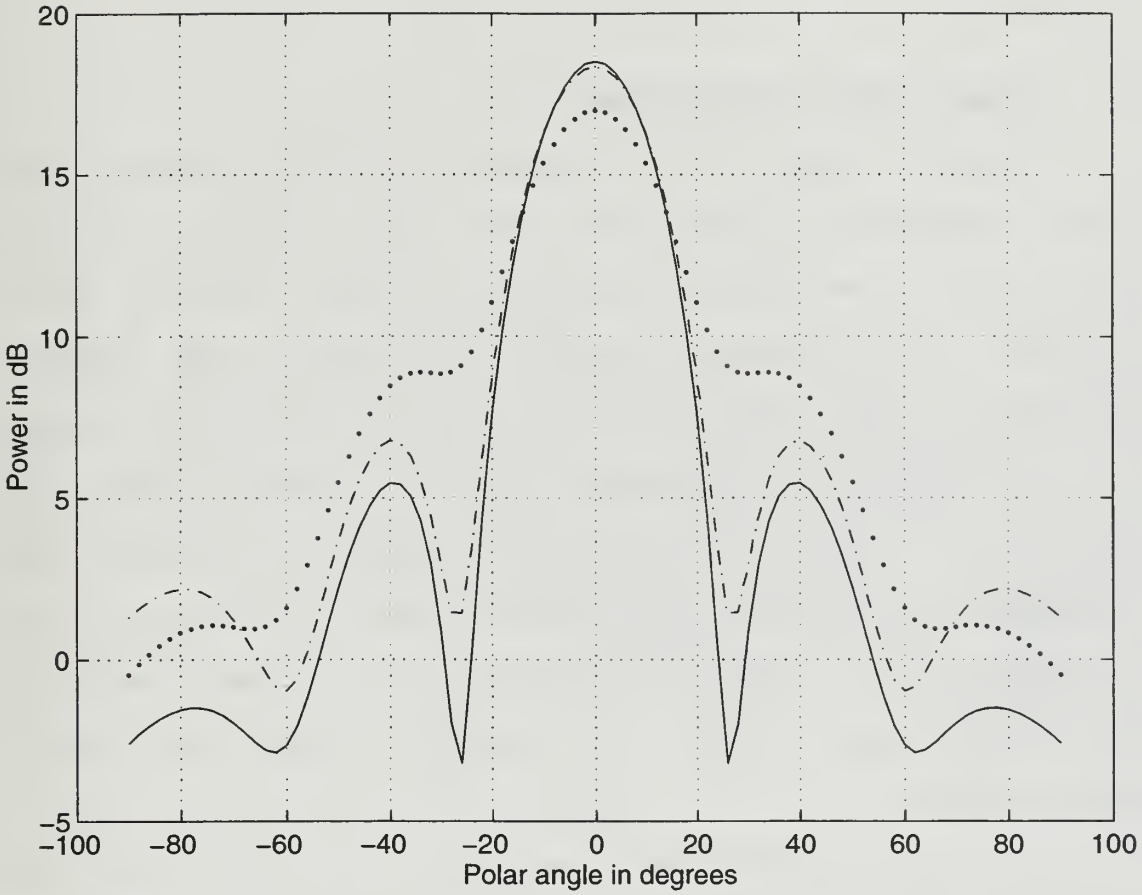

Figure 46. Radiation patterns for the geometries of Figures 7 (solid line), Figure 42 without phase correction (dotted line) and Figure 42 with phase correction (dash-dotted line) when the main beam is at 0 degrees.

improvement as far as the level of the sidelobes is concerned. Note that even though the array factor has been steered to -60 degrees, the beam maximum appears to be at -57 degrees due to roll-off of the dipole element pattern (Figure 47).

E. PLANAR ARRAY CALCULATIONS

A planar array, or more generally, a two dimensional array, provides a beam whose width and direction can be controlled in two principal planes. A 5 by 5 array is shown in Figure 48. The spacing along the x axis is the same as the linear array (0.4 wavelength) while the spacing along the y axis is 0.55 wavelength and the height above the ground plane is 0.15 wavelength. The radiation patterns for broadside and scanned conditions are shown in Figures 49 and 50 respectively. Again the distortion of the main beam for the scanned case is due to the element pattern roll-off at large angles.

As it has already been mentioned, the most important advantage of such a planar array is the ability to steer the beam pattern in two dimensions. The next step is to perform beam steering to a direction $\theta = -25^{o}$ and $\phi = 45^{o}$ by phase shifting each element in the array. The results are shown in Figure 51 for ϕ and θ-polarizations respectively.

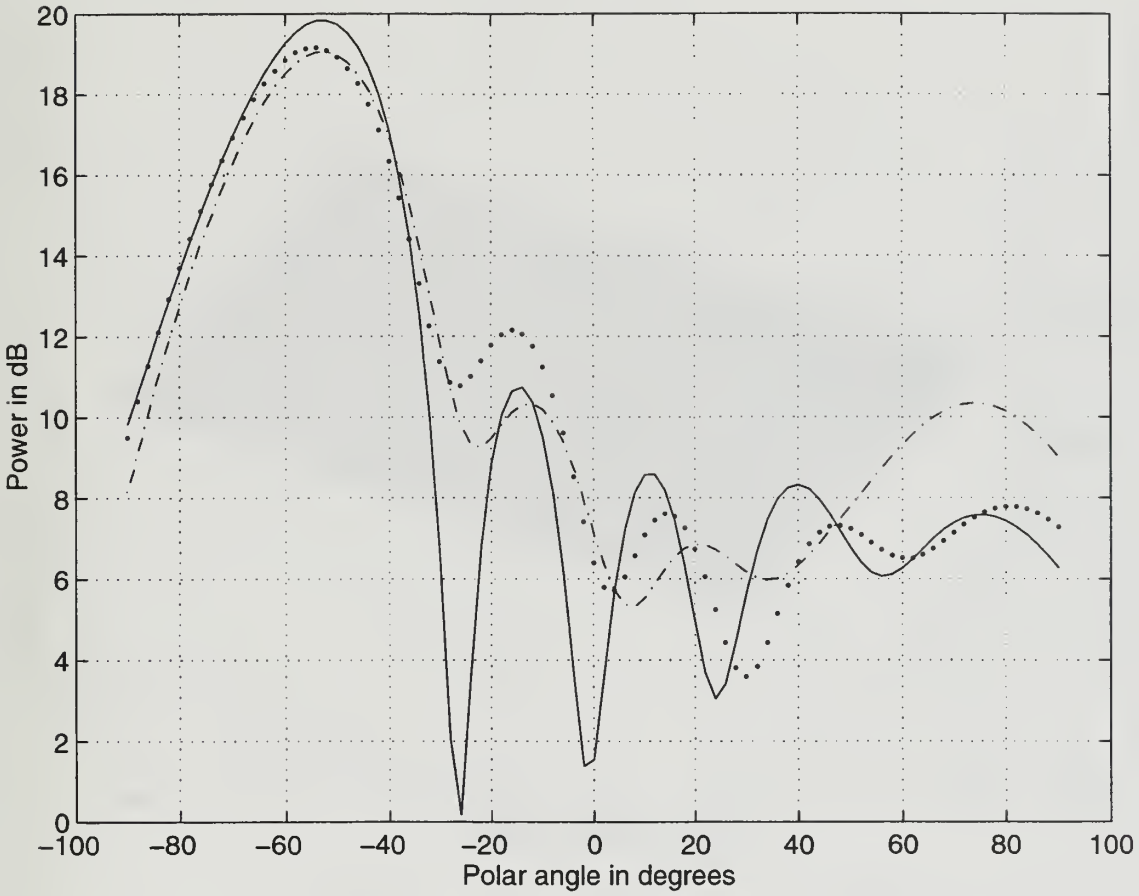

Figure 47. Radiation patterns for the geometries of Figure 7 (solid line), Figure 42 without phase correction (dotted line) and Figure 42 with phase correction (dash-dotted line) when the main beam is at -60 degrees.

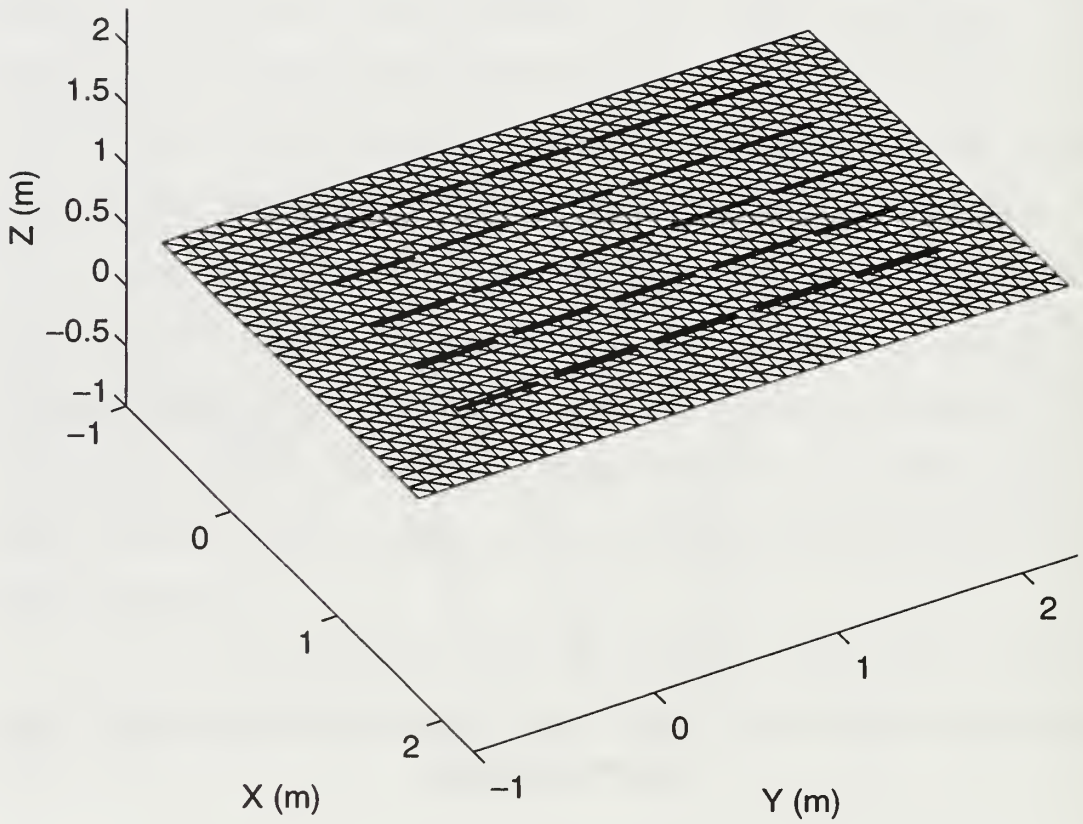

Figure 48. Five by five array over flat ground plane.

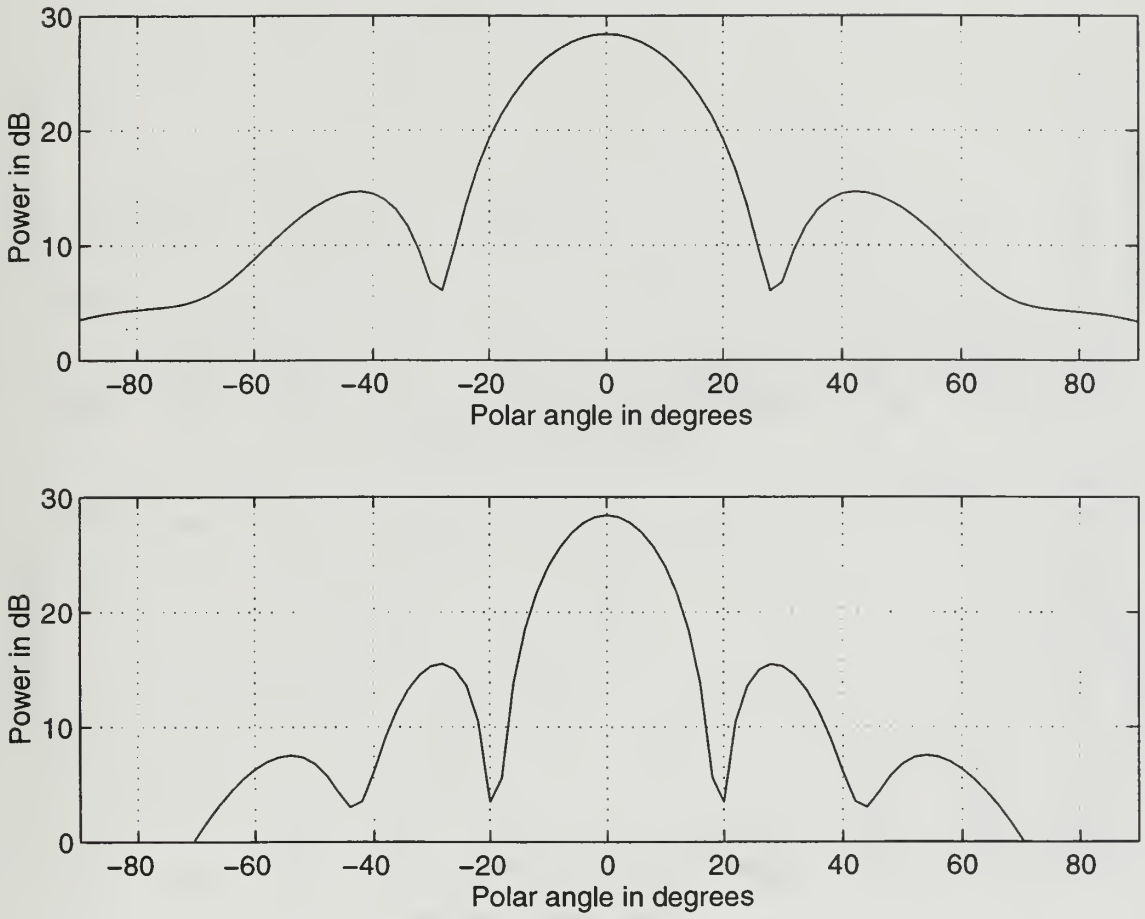

Figure 49. Radiation patterns for the five by five array for broadside conditions. Top: ϕ-polarization for $\phi = 0^o$. Bottom: θ-polarization for $\phi = 90^o$.

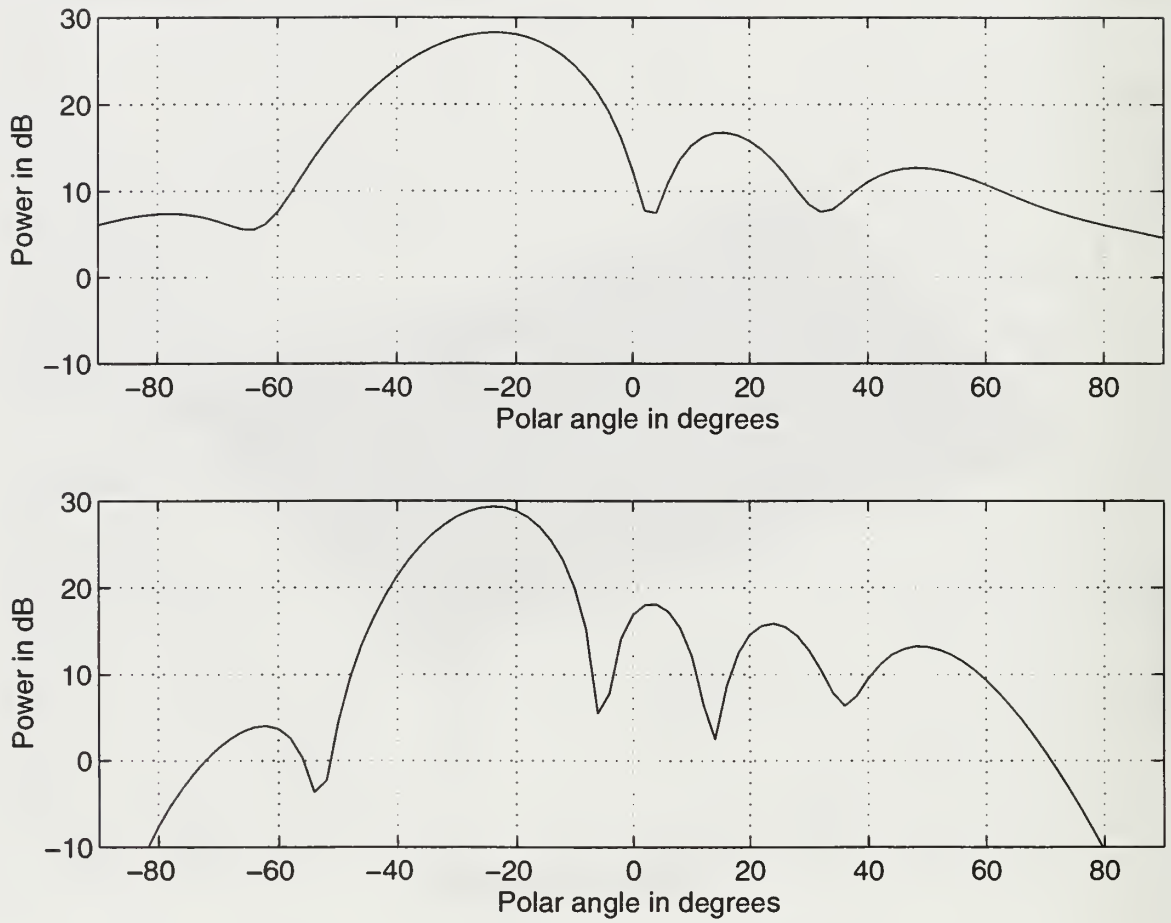

Figure 50. Radiation patterns for the five by five array for beam steered at $\theta = -25^o$. Top: ϕ-polarization for $\phi = 0^o$. Bottom: θ-polarization for $\phi = 90^o$.

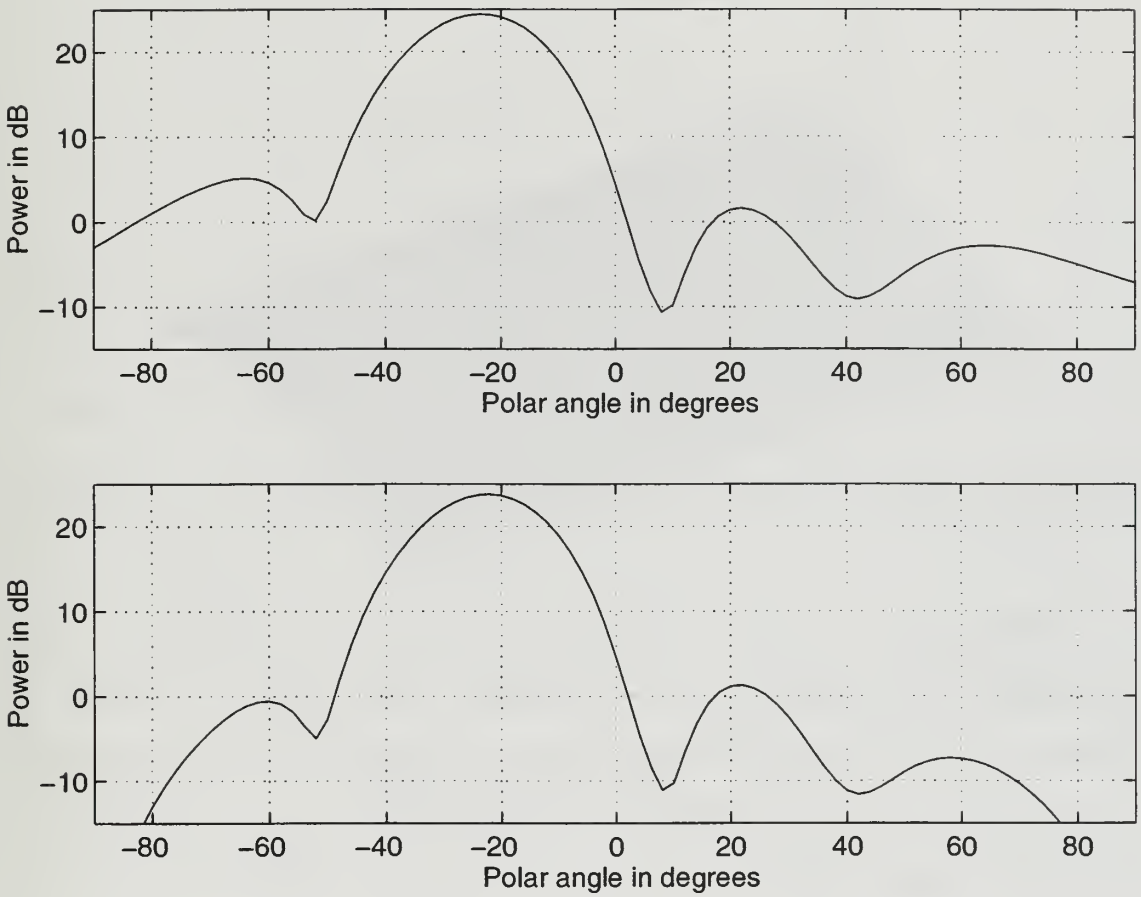

Figure 51. Radiation patterns for the five by five array for main beam steered to $\theta = -25^{o}$ and $\phi = 45^{o}$. Top: ϕ-polarization; Bottom: θ-polarization.

The directivities for the various scan conditions are shown in Table 2 for the five by five array.

Scan angle (degrees)		Directivity (dB)
ϕ	θ	
0	0	19.1025
0	45	18.6677
90	25	18.5655
45	25	18.5443

Table 2. Maximum directivity for 5 by 5 array as a function of scan angle.

Finally, the two dimensional array is curved in one dimension to conform to a cylinder. The array is shown in Figure 52. The patterns are shown in Figure 53 and compared to the flat array results. Contour plots are presented in Figures 54 and 55.

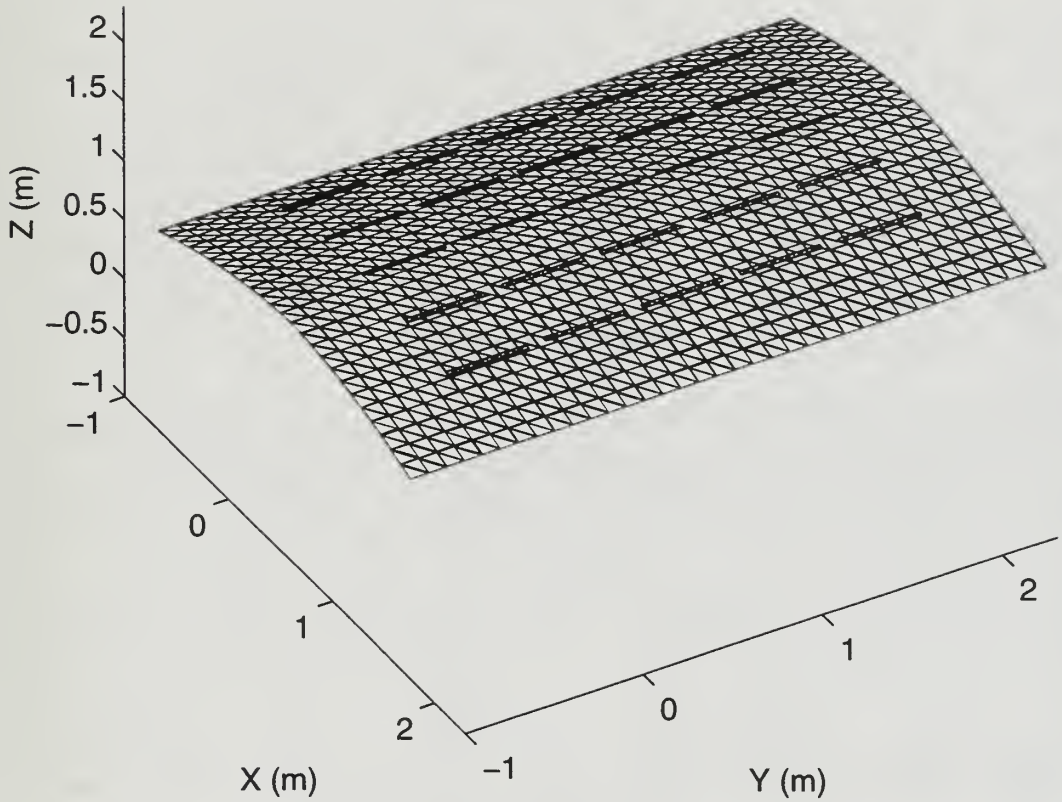

Figure 52. Curved five by five array over ground plane.

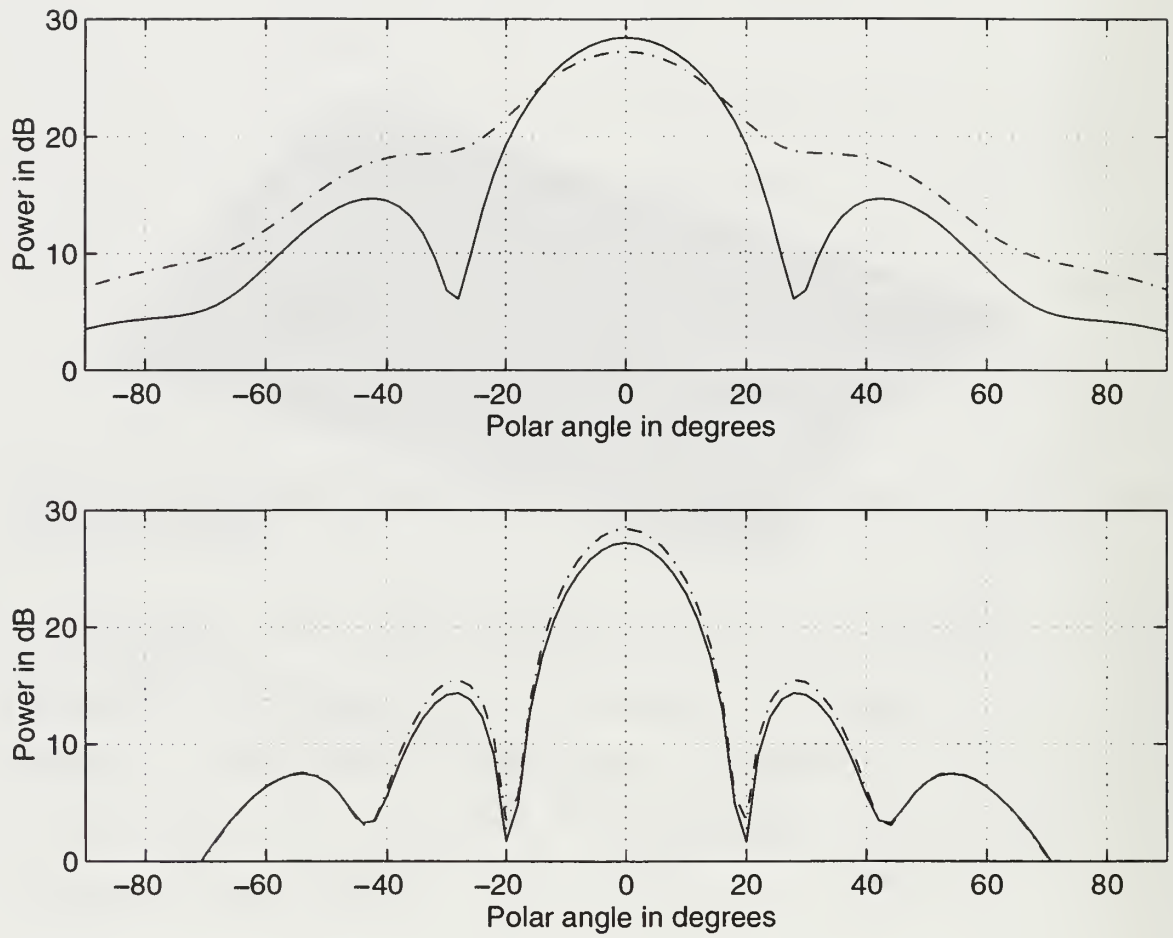

Figure 53. Radiation patterns for the five by five array with flat (solid line) and curved (dash-dotted line) geometry. Top: ϕ-polarization for $\phi = 0^o$. Bottom: θ-polarization for $\phi = 90^o$.

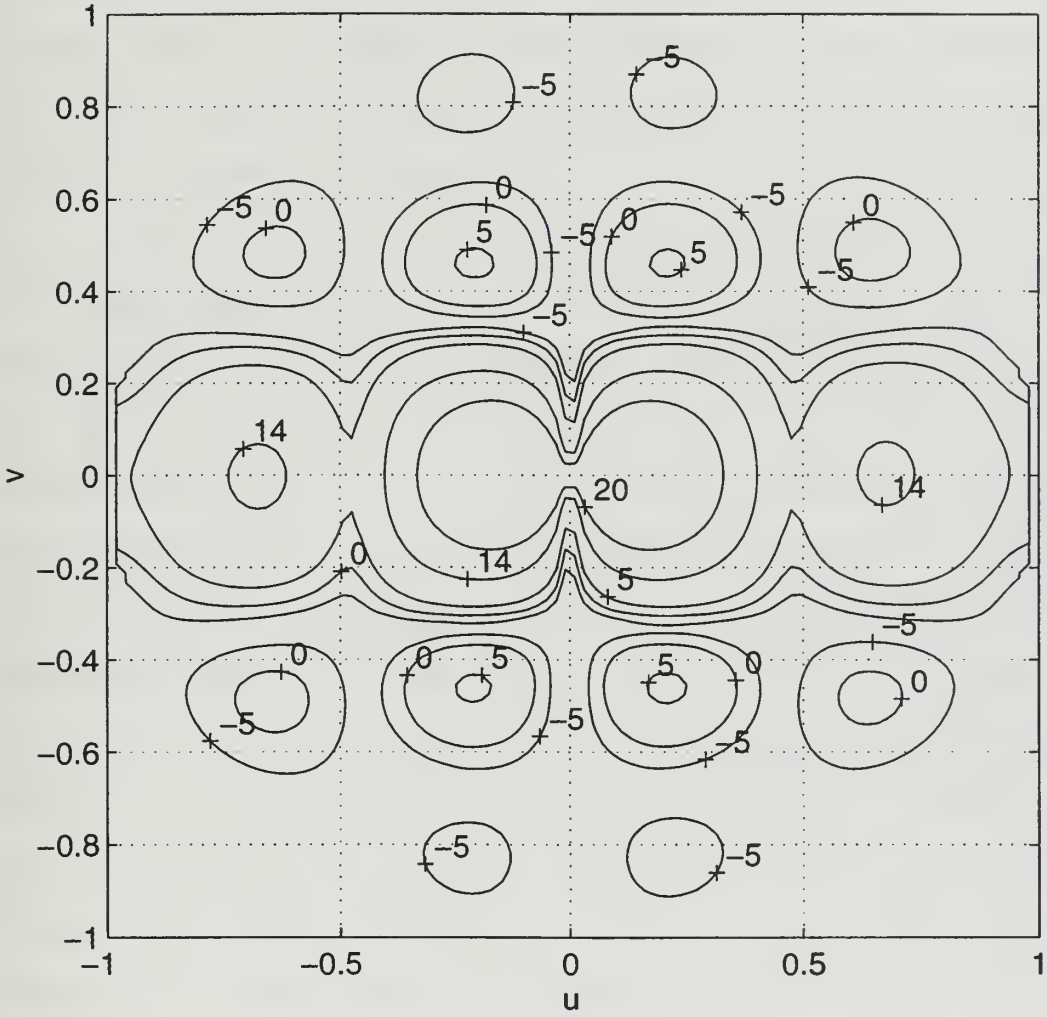

Figure 54. Contour plot (in dB) of the radiation pattern for the geometry of Figure 48.

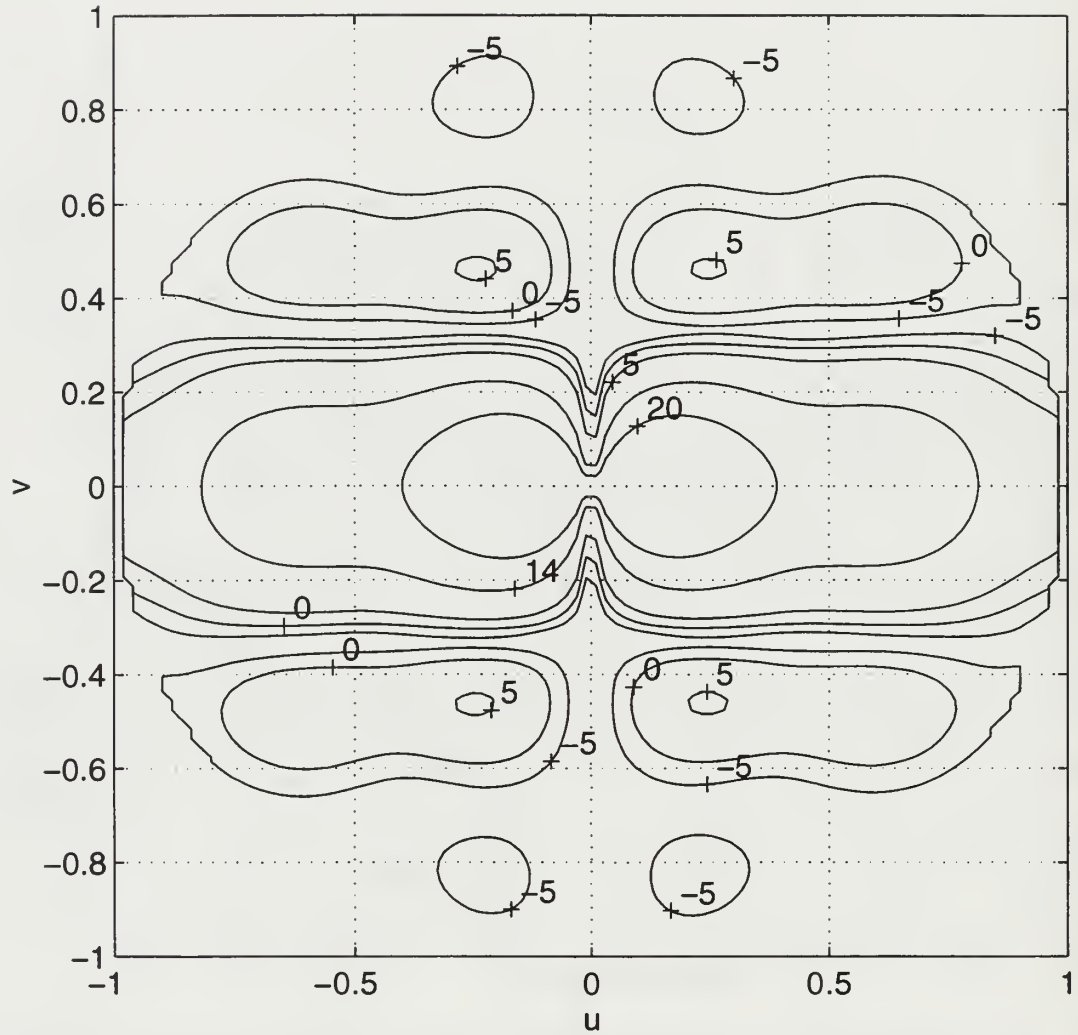

Figure 55. Contour plot (in dB) of the radiation pattern for the geometry of Figure 52.

V. CONCLUSIONS

In the previous chapter, the performance of finite phased arrays over finite ground planes has been investigated. The effect of ground plane shape and curvature have also been examined. The data were generated using the method of moments code **patch**.

The termination of the array leads to an increase in the wide angle sidelobes because of the mutual coupling and scattering from the ground plane edges. Collectively these are referred to as the "edge effect," and it is clearly illustrated by plotting the individual element patterns. The end elements of the array displayed narrow asymmetric pattern shapes, which cause a high gain loss as the beam is scanned. This occurred even when the ground plane was infinite. The termination of the ground plane has little effect on the main beam gain unless the beam is scanned far from broadside. This assumes that the ground plane extends beyond the edge elements of the array. (A common rule of thumb is ½ past the last element.)

Since the ground plane edge scattering is the source of higher sidelobes, it is possible to control the sidelobe location by tilting the edge. This was demonstrated by using a ground plane with triangular shaped edges. The principal

plane sidelobe level was reduced at the expense of the off-principal plane sidelobe level.

Another configuration that this study examined was an antenna mounted on a curved surface (e.g., aircraft wing). As it has been shown, the effects include a degradation in gain because the curvature is equivalent to adding a phase error. A phase correction was introduced to each element in order to improve the directivity.

The pattern data has shown that the scattering from the ground plane edge is a more important contributor to the increase in the wide angle sidelobes than the mutual coupling. Future studies should investigate methods to reduce this scattering using various edge treatments. Another possible approach is to intentionally mismatch the edge elements in the array. The loads would be chosen so that the scattering due to the mismatch would add destructively with the scattering from the ground plane edge.

The effect of amplitude tapering should also be investigated. For small arrays Chebychev distributions are commonly used [Ref. 5]. The edge elements are excited at a much lower level than the center elements in the array, leading to a lower ground plane edge illumination and, thus, potentially reducing the edge effect.

LIST OF REFERENCES

1. Hall, P. S., "Survey of design techniques for flat profile microwave antennas and arrays," *The Radio and Electronics Engineers*, Vol 48, No 11.

2. Shavit, R., "Circular Polarization Microstrip Antenna on a Conical Surface," *IEEE Transactions on Antennas and Propagation*, Vol. 45, NO. 7, July 1997

3. Jin, J. M., "Calculation of Radiation Patterns *of Microstrip Antennas on Cylindrical Bodies of Arbitary Cross Section," IEEE Transactions on Antennas and Propagation*, Vol. 45, NO. 1, January 1997

4. Jonson, W., et al, "Patch Code Users' Manual," Sandia Report, Sand87-2991, Sandia National Laboratories, Albuquerque, NM, May 1988.

5. Colin, R. E., "Antennas and Wave Electromagnetics," *Second Edition*, Addison-Wesley, Inc., New York, NY, 1992

INITIAL DISTRIBUTION LIST

1. Defense Technical Information Center 2
   8725 John J. Kingman Rd., STE 0944
   Ft. Belvoir, Virginia 22060-6218

2. Dudley Knox Library.....2
   Naval Postgraduate School
   411 Dyer Rd.
   Monterey, California 93943-5101

3. Chairman, Code EC.....1
   Department of Electrical and Computer Engineering
   Naval Postgraduate School
   Monterey, California 93943-5121

4. Prof. David C. Jenn, Code EC/Jn.....1
   Department of Electrical and Computer Engineering
   Naval Postgraduate School
   Monterey, California 93943-5121

5. Prof. Phillip E. Pace, Code EC/Pc.....1
   Department of Electrical and Computer Engineering
   Naval Postgraduate School
   Monterey, California 93943-5121

6. Embassy of Greece.....1
   Naval Attache
   2228 Massachusetts Ave., NW
   Washington, DC 20008

7. Ioannis E. Daniil.....2
   Konstantinoupoleos 56-60 St.
   Vironas
   Greece